Quaternary Science Reviews 276 (2022) 107292

Contents lists available at ScienceDirect

Quaternary Science Reviews

journal homepage: www.elsevier.com/locate/quascirev

Temporal variability in the relative strength of external drivers controlling ecosystem succession in a coastal wetland near Bayou Lafourche, southeast Louisiana, USA

Junghyung Ryu [a, *], Kam-biu Liu [a], Terrence A. McCloskey [b]

[a] Department of Oceanography and Coastal Sciences, College of the Coast and Environment, Louisiana State University, Energy, Coast & Environment Building, Baton Rouge, USA
[b] St. Margarets Village, Mile 32 Hummingbird Highway, Belize, Central America

ARTICLE INFO

Article history:
Received 23 September 2021
Received in revised form
16 November 2021
Accepted 21 November 2021
Available online xxx

Handling Editor: I Hendy

Keywords:
Avicennia
Louisiana wetland
Pollen
External forcing agents
PCA
XRF

ABSTRACT

The coastal wetlands of Louisiana are extremely dynamic due to their location on the edge of the continent, the heavy but spatially and temporally variable influence of the discharge of the Mississippi River, and the effects of both chronic (sea-level rise, coastal retreat) and abrupt (hurricanes, lobe switching) stressors. In these coastal wetlands the timing and mode of ecological succession can result from a variety of external factors and vary from sudden to gradual. This paper uses a palynology-based multi-proxy analysis of sediment cores retrieved from a small pond on a mangrove-dominated island in Bay Champagne near Port Fourchon, Louisiana to describe and date the successive ecosystems that have covered this site since 4000 BP and applies a PCA-based interpretation to infer the drivers responsible for each shift. During the late Holocene, the most important controlling agents have been the Mississippi River delta development, sea-level rise, climatic variability, shoreline retreat, tropical cyclones, and, more recently, anthropogenic effects. These processes have progressively transformed the site from a freshwater to a saline environment, consisting of four distinct ecosystems: a *Taxodium-Nyssa* freshwater forest (4.0–1.3 cal yr BP), a *Typha-Bacopa* freshwater deltaic-lake (1.3–0.7 cal yr BP), an intermediate and brackish marsh (0.7–0.2 cal yr BP), a *Spartina*-dominated saline marsh (since 0.2 cal yr BP), and a short-stature *Avicennia* forest since the early 1900s. The Mississippi River delta cycle (lobe switching) was the dominant driver of ecosystem changes early in the site's history, while relative sea-level rise, shoreline retreat, tropical cyclones, climate, and anthropogenic effects have been the main drivers since the 19th century.

1. Introduction

Containing one of the world's largest deltas, coastal Louisiana has experienced rapid land loss (5197 km^3 since the 1930s; Couvillion et al., 2017). This has resulted in the inland migration of both infrastructure and the human population (Monte, 1978), with major negative impacts on the local, regional, and national scale. This coastal retreat is due to a variety of factors, including eustatic sea-level rise (SLR), subsidence, and anthropogenic activities. The standard ecological progression in such locations is predictable, as relative sea-level rises, salt marsh transitions to open water, fresh marsh transitions to salt marsh, and the bottomland hardwood forest retreats landward. However, the timing and rapidity of these ecosystem changes and the recent trend toward the replacement of *Spartina*-dominated salt marsh with black mangrove (*Avicennia germinans*) along the southernmost sections of the coast are controlled by several factors (Perry and Mendelssohn, 2009; Alleman and Hester, 2011; Krauss et al., 2014), all of which must be fully understood in order to develop workable societal responses to this transgression. Millennial-scale paleo-environmental reconstructions can aid this understanding by establishing long-term records of ecological changes and inferring the external factors controlling the timing and direction of ecosystem shifts. Unfortunately, such paleoecological studies are almost entirely lacking for coastal Louisiana.

Palynology-based paleoenvironmental studies are typically

* Corresponding author.
E-mail addresses: jhrainlv7@gmail.com (J. Ryu), kliu1@lsu.edu (K.-b. Liu), tamccloskey2014@gmail.com (T.A. McCloskey).

https://doi.org/10.1016/j.quascirev.2021.107292
0277-3791/

conducted in morphodynamically stable environments such as inland lakes (Liu, 1990; Sugita, 1993) in order to reduce the number of controlling variables. Given constant geological background parameters, the changes of pollen percentages can be correlated to a single factor, usually climate. However, the dynamic geological conditions that dominate coastal Louisiana create a much more complicated scenario. Multiproxy analyses can be employed to help distinguish natural and anthropogenic factors and identify the effects of such non-climatic factors as the delta lobe-switching associated with the Mississippi River, the frequency of hurricane landfalls, local salinity levels, coastal subsidence, and local and eustatic SLR.

Recognizing that the relative importance of these different factors varies both temporally and spatially is an essential step in untangling the ecosystem successions on deltaic coasts. In this study, we reconstruct the environmental history of a coastal site over the last 4000 years, highlighting our view that the dominant external driver forcing ecosystem changes has varied over time.

2. Study site

Louisiana marshes are one of the major components of the extensive wetlands occurring along the Gulf coast. Louisiana wetlands contain over 57 000 km^2 of marshland (Couvillion and Beck, 2013), including large disjunct areas of freshwater marsh and a vast, practically unbroken expanse of saline "wet prairie" of brackish and saline-water marshes (Penfound and Hathaway, 1938).

Bay Champagne is located in southeastern Louisiana along the southernmost coast of Lafourche Parish along the Caminada-Moureau Headland near Port Fourchon (Fig. 1C), bounded on the north by Bayou Lafourche and on the south by the Gulf of Mexico. Bay Champagne is a shallow (<2 m in depth), semi-circular, enclosed coastal lake separated from the sea by a predominantly sand barrier <1 m in height (Authority, 2012; Dartez et al., 2020). Shoreline retreat of the Caminada-Moureau Headland has been rapid during the instrumental period, with a rate of 12.5 m/yr from 1884 to 2002 and a rate of 2.6 m/yr from 1988 to 2002 (Penland et al., 2005). The Caminada-Moureau coast has retreated approximately 1.5–2 km since 1884 (Kindinger et al., 2013, Fig. 1C) as a combined result of hurricanes, storm surge, and RSLR (Naquin et al., 2014; Dietz et al., 2018) as well as human impacts (e.g., beach nourishment projects; Dietz et al., 2018). As a result, Bay Champagne's surface area has been reduced by approximately 48% since 1983 (Dietz et al., 2018).

2.1. Geological setting

During the Holocene, the Mississippi River has created and abandoned several successive distributaries and their associated delta lobes (Coleman et al., 1998). This process referred to as the "delta cycle", has created a sequential series of regressive and transgressive depositional systems consisting of the six major delta complexes, and more than 16 smaller subdeltas (Kolb et al., 1958; Saucier, 1968; Penland et al., 1988, Fig. 2), resulting in an extremely dynamic coastal morphology. As a delta develops it fills the lower alluvial valley with sediment, making the path of the river to the Gulf outlet less hydrologically efficient. Eventually, the river diverts to a new channel upstream, and discharges down the new path, building a new delta in a new location, leading to subsidence of the abandoned lobe due to the lack of fluvial input. This process is known as "lobe switching". During a maximum development of the delta, swamp and marsh ecosystems become more abundant as the subaerial delta plain becomes discontinuously subaqueous, creating diverse geomorphological features and increasing

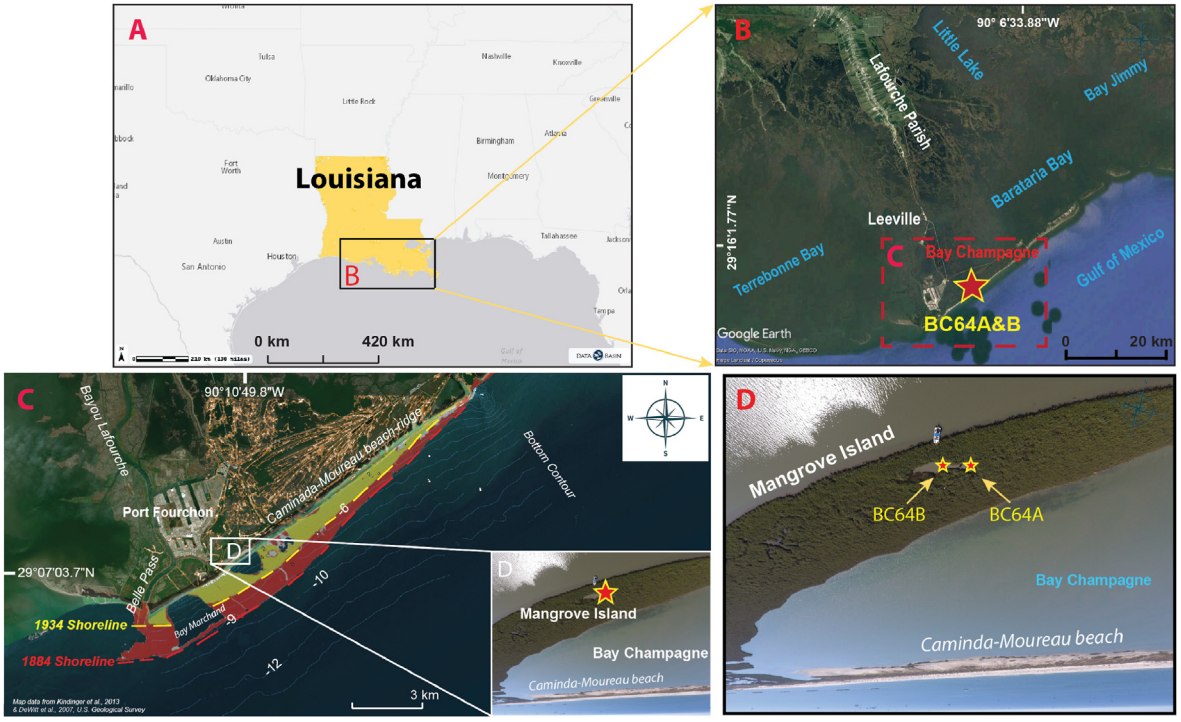

Fig. 1. Maps of study site. (A) The state of Louisiana is marked in yellow. (B) The red-dashed box marks Bay Champagne area and coring sites (BC64A&B) are indicated by a star. The proximity of the study site to the Gulf of Mexico, Terrebonne Bay, Barataria Bay, and Bay Jimmy is displayed. (C) Recent coastal retreat as demonstrated by the 1884 (red) and 1934 (yellow) shorelines. (D) Coring sites (BC64A&B) are indicated by stars and a mangrove island and the Caminada-Moureau beach and beach-ridge are displayed. The shoreline evolution was made using Global Mapper v.18. and data from Kindinger et al. (2013); and DeWitt et al. (2007). The maps were produced using Data Basin (A), Google Earth (B, D), ArcGIS 10.3 (C). (For interpretation of the references to color in this figure legend, the reader is referred to the Web version of this article.)

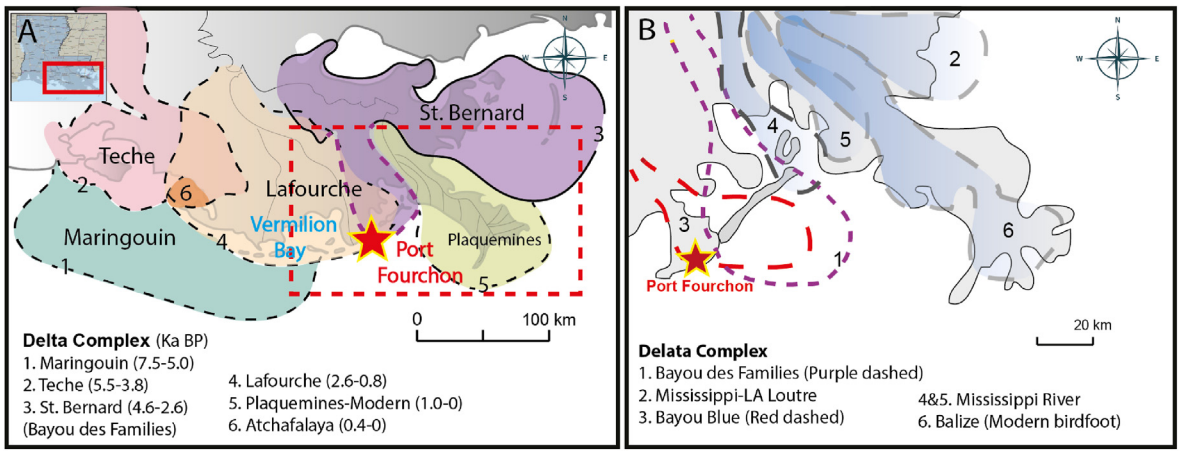

Fig. 2. (A) Holocene delta complexes of Mississippi delta. Port Fourchon is indicated with a star. The colored areas indicate the extended deltaic plans. (B) The complexes of St. Bernard (Bayou des Families: purple dashed) and Lafourche (Bayou Blue: red dashed) deltas. The red star marks the coring site. The map was modified from Flocks et al. (2006) based on data from Frazier (1967) and Levin (1991). (For interpretation of the references to color in this figure legend, the reader is referred to the Web version of this article.).

topographic heterogeneity, resulting in a wider spectrum of hydrogeomorphic zones (Twilley et al., 2019).

Recent studies (Flocks et al., 2006; Törnqvist et al., 2008; Blum and Roberts, 2012) have detailed the histories of St. Bernard and the Lafourche delta complexes, the delta complexes that mainly impact our study site. During 4600–2000 BP, the St. Bernard delta complex prograded to the southwest, establishing multiple distributary channels leading to the Gulf Coast (Frazier, 1967; Levin, 1990) (SI1). This delta formed a typical inland sequence of facies overlain by a thick aggradational deposit. The St. Bernard delta complex was active in the study region between 4600 and 2600 BP (Levin, 1990) until the delta switched its major distributaries to the east between 3000 and 1900 BP (Flocks et al., 2006). Meanwhile, deposits from the Lafourche delta complex started to occupy the western portion of the study region ~2600 BP (Fig. 2). Although the active periods of Lafourche delta complex vary in different studies (Frazier, 1967; Saucier, 1968; Levin, 1990; Shen et al., 2015; Chamberlain et al., 2018; Bomer et al., 2019), it is obvious that the major distributaries around the study site were redirected from St. Bernard complex to the Lafourche course rather than the other way around (Hijma et al., 2017; Bomer et al., 2019).

2.2. Ecological setting

The current Louisiana coastal ecosystems spatial zonation pattern transitions [moving seaward] from bottomland and swamp forest, to freshwater marsh, to intermediate/brackish marsh, to salt marsh, to mangrove at the coast. The location of the ecotones between the five wetland types is primarily dependent upon salinity, which is basically controlled by three factors: proximity to the sea, elevation, and freshwater input. The study site is at the far seaward end of the zonation in a shallow pond surrounded by black mangrove (*Avicennia germinans*), cordgrass (*Spartina alterniflora* and *patents*), and black needlerush (*Juncus roemerianus*), situated on a mangrove island along the northern edge of Bay Champagne (Fig. 1D).

2.3. Relative sea-level rise (RSLR)

RSLR is one of the main natural factors driving the current oceanic transgression that results from a combination of eustatic sea-level rise and subsidence. The magnitude of RSL varies across the Gulf of Mexico (GOM) [Gonzalez and Törnqvist, 2009) both temporally and spatially. Temporally, numerous sea level index points indicate that RSL rise in the Mississippi River delta region was particularly rapid (~3.5 mm/yr) prior to ~7000 BP, and then dropped rather abruptly to values of ~1.5 mm/yr (Tö;rnqvist et al., 2004). Spatially, RSL currently varies from 5 to 12 mm/yr for southern Louisiana (Jankowski et al., 2017; Raynie et al., 2020). The study region is currently experiencing the RSL rise of ~10 mm/yr (Jankowski et al., 2017).

2.4. Tropical cyclones

Coastal Louisiana has experienced frequent strikes from tropical cyclones, including major hurricanes such as Betsy (1965), Camille (1969), Katrina (2005), Laura (2020), and Ida (2021) during both the instrumental and paleo periods (Roth, 2010). Such powerful storms can result in shoreline retreats and destruction/alterations to pre-existing ecosystems (Control and Prevention, 2005; McCloskey et al., 2018). Although the coastal morphology and ecosystem changes resulting from historical storms have been documented (Guntenspergen et al., 1995; Turner et al., 2006; Törnqvist et al., 2007; Tweel and Turner, 2012), the effects of earlier paleo-storms have not been determined.

2.5. Mangroves

Under the current warming climate, the three Gulf mangrove species, *Rhizophora* (red mangrove), *Laguncularia racemosa* (white mangrove), and *Avicennia germinans* (black mangrove), have been migrating northward along the GOM, with their northern limit primarily controlled by winter temperatures although interactions between hydroperiod, sedimentation, elevation, salinity, and nutrient levels influence the precise limiting points (Patterson and Mendelssohn, 1991; Osland et al., 2013). Osland et al. (2020a, 2020b) identified that temperature thresholds of black mangroves for leaf damage are near −4 °C, with temperature thresholds for mortality being closer to −7 °C. As a result, recently black mangroves have expanded rapidly into salt marshes in the northern GOM (Patterson et al., 1993) with black mangroves having reached Louisiana as early as the 1900s (Penfound and Hathaway, 1938), although the current rapid expansion began around the 1990s (Patterson and Mendelssohn, 1991). Human activities such as dredging, canal digging, and the construction of structures in estuaries have also impacted the expansion/distribution of black

mangroves in Louisiana (Monte, 1978). The expansion of red and white mangroves has been limited to the coast of Texas and Florida (Montagna et al., 2007; Yao et al., 2015).

2.6. Climate (medieval warm period (MWP), Little Ice Age(LIA))

Climatic conditions in the GOM during the Late Holocene have varied between wet/warm and cold/dry periods, with the wet/warm periods increasing evaporation over the GOM, enhancing precipitation over North America, with reverse conditions occurring during cold/dry periods (Flannery, 2008). This oscillation has resulted in large temporal variability in the volume of freshwater discharge through the Mississippi River, with subsequent impacts on geological and ecological conditions along the coastal wetlands.

2.7. Drivers

In coastal Louisiana, the ecosystem/vegetation type occurring at any specific location, as well as the timing and details of ecological changes occurring at the site, are controlled by all of these background conditions. Those background parameters, in turn, are controlled by a large number of independent drivers, which can vary in scale from global (climate, eustatic sea level), to regional (subsidence), to quasi-regional (lobe switching), to local (proximity to a distributary and extent of water/gas extraction). This paper examines the long-term ecological history of a specific site, highlighting the fact that ecological change has been driven by different drivers at different times. This study is an attempt to emphasize that the relative strength of the different forcing agents has not remained constant over time and that understanding the ecological response at any specific site at any specific time requires the accurate identification of the dominant external agent(s).

3. Material and methods

In September 2017 and March 2018, 2.14 m (BC64A) and 3.72 m (BC64B) sediment cores were retrieved using a push corer and vibra corer respectively, from a small pond on a black mangrove-dominated island (29°7′3.47″N, 90°10′50.64″W, 29°7′3.43″N, 90°10′50.78″W) within Bay Champagne near Port Fourchon, Louisiana (Fig. 1). The cores were transported in a vertical position to the Department of Oceanography & Coastal Sciences, Louisiana State University, where they were stored in a refrigerated room (4 °C). When opened, the cores were split longitudinally, photographed, and described with coloration based on the Munsell color chart (Malacara, 2011).

3.1. Chronology

The core chronology was developed through radiocarbon and germanium γ-spectrometer (^{210}Pb and ^{137}Cs) dating techniques. The radiocarbon chronology was based on seven samples of organic material (plant debris) intercalated between sand and silt deposits. The samples were carefully collected above a relatively hard substrate since the Mississippi deltaic sediment mainly consists of sand, silt, and clay instead of an incompressible substrate (i.e., gravel and bedrock). The samples were sent to International Chemical Analysis, Inc. for accelerator mass spectrometry (AMS) dating. The 95% confidence intervals for calendar years BP were determined under the assumption of a Gaussian distribution on the ^{14}C age scale (Christen and Pérez, 2009). Calendar age points using the IntCal 13.14C calibration estimate for depths were based on the weighted average of all age-depth curves (Talma and Vogel, 1993; Stuiver et al., 1998). An age-depth model was developed using Clam v2.2 (Blaauw, 2010).

^{137}Cs and ^{210}Pb activities were measured from core BC64B at 1–2 cm intervals from a depth of 0–40 cm in a low-energy germanium γ-spectrometer in Dr. Carol Wilson's lab at LSU, following the methods of Wilson and Allison (2008). The sediment samples were dried for 36 h, then ground using a mortar and pestle, and packed in 60 mm test tubes (well geometry) (Wilson and Allison, 2008). All samples were sealed with epoxy to prevent ^{222}Rn loss and set aside for at least 21 days to allow for ingrowth to reach secular equilibrium for ^{210}Pb, then counted for 1–2 days. Activities were calculated following the methods detailed in Allison et al. (2007). The results of gamma-ray activities were reported in decays per minute per gram of dry sediment (dpm/g, 1 dpm = 60 Bq). A linear regression of the natural logarithm of excess ^{210}Pb (^{210}Pb$_{xs}$) with depth below 20 cm was applied to examine the sediment accretion rate (SAR; (Nittrouer and Sternberg, 1981; Wilson and Allison, 2008). ^{137}Cs activity was analyzed to detect the initiation of ^{137}Cs fallout resulting from thermonuclear weapon tests (1954 CE) and the year of maximum fallout in the northern hemisphere (1963 CE). ^{137}Cs accumulation rate was calculated based on the 1963 peak and onset of the atmospheric hydrogen bomb testing (1954).

3.2. Sedimentary (LOI and granulometry)

Loss-on-ignition (LOI) analysis was performed at 1 cm resolution down the center of the cores to determine water, organic, carbonate, and residual (mainly siliciclastic) content, following the procedure of Dean (1974) and Liu and Fearn (2000).

For grain-size analysis, sediment samples were taken at 5–15 cm intervals in both cores at sample depths corresponding to abrupt sedimentary shifts as marked by changes in LOI percentages. For both cores particles >2000 μm were removed by a dry-sieve while particles <2000 μm were wet-sieved (Gee and Or, 2002) through various sieve numbers (e.g., 10, 40, 200) standard sieves, at least three times. Median grain size is reported for each sample.

Twelve additional samples (~1 g of dry material) were collected from BC64B and analyzed using a Beckmann-Coulter laser diffraction particle size analyzer (Model LS 13 320). The samples were pretreated with hydrogen peroxide and hydrogen chloride to remove organic and carbonate material and then sonicated to disaggregate particles prior to transfer to the laser chamber (Xu et al., 2014). Mean grain size, sorting, skewness, kurtosis, sample type, textural group were calculated using GRADISTAT (Blott and Pye, 2001), with mean grain size reported for each sample. To construct complete core lithology, visual and fossil analyses were performed at 5 cm intervals throughout the core. Fossils (plant debris and shells) and soil texture were analyzed using conventional methods (Watts and Winter 1966; Wells, 1976; Shirazi and Boersma, 1984; Shirazi et al., 1988).

3.3. X-ray fluorescence

To determine the hydro-environmental conditions, the cores were scanned at 2-cm intervals with an Innov-X Delta Premium DP-4000 X-ray fluorescence (XRF) analyzer which measures fluorescence to estimate concentrations (ppm) of 32 elements. The XRF unit utilizes high-resolution spectral analysis in the 8–60 keV region. Calibration was performed with the National Institute of Standards and Technology (NIST) standards (2710a and 2711a). Based on previous studies, the elements Ca, Sr, and Cl were selected as indicators of marine conditions, Zr, Ti, K, and Mn as terrestrial indicators, and Br as an organic indicator (McCloskey et al., 2017; Ryu et al., 2018, 2021b). Cl/Rb and Zr/Rb ratios were calculated and are presented as proxies for the relative strength of marine (Cl/Rb) (Liu et al., 2014) and fluvial (Zr/Rb) influences, respectively. Rb was

used to minimize the influence of grain size variability as Rb has been used as a suitable detrital divisor (the element that is being divided by) (Croudace et al., 2006; Rothwell and Rack, 2006).

3.4. Pollen analysis

Pollen and charcoal were analyzed from BC64B at 2–5 cm intervals throughout the core. The eighty sediment samples (1.8 ml each) were processed using conventional methods (Faegri et al., 1964; Liu et al., 2008), with exotic *Lycopodium* tablets added to determine pollen concentration. A minimum of 300 pollen grains was counted for each sample. Published pollen guides (Godwin, 1934; Wodehouse, 1937; McAndrews et al., 1973; Faegri et al., 1989; Willard et al., 2004) were used to aid identifications. *Spartina* pollen was distinguished from the pollen of other common wetland Poaceae plants such as *Phragmites* based on size and pore diameter as *Spartina* pollen is generally larger (maximum dimension 33.0–42.0 μm) than *Phragmites* pollen (maximum dimension between 21.9 and 26.5 μm), and has a larger pore (pore diameter of 3.8 μm versus 1.5–2.4 μm for *Phragmites*) (Willard et al., 2004). Pollen diagrams were graphed using C2 software (Juggins, 2007)). Additionally, charcoal fragments >10 μm were counted. Macrofossil analysis was conducted at a 5 cm interval throughout the core. Foraminifera (*Ammonia*) tests were analyzed by conventional methods (Boonstra et al., 2015) to identify marine incursions.

3.5. Statistical analysis

Geochronological correlations between the two cores (BC64A and BC64B) were determined using *R* software packages (e.g., "tidyverse", "ggpmisc") for calculations of r^2-and *p*-values (Pongrac et al., 2020) in linear regression (Wickham et al., 2019; Pongrac et al., 2020). Potential correlations between elemental concentrations and four taxonomic groups (floodplain trees, tidal freshwater herbs, inland herbs, and saline herbs) were tested by means of principal component analysis (PCA) (Hicks and Birks, 1996) using *R* software packages (e.g., "rioja", "factoextra", "FactoMineR"; Ryu et al., 2021b). In order to summarize and visualize the relationships between ecosystem type and geochemical conditions biplots were developed for eighty-one samples taken at 5 cm intervals from 372 cm to 0 cm using averaged elemental concentrations between the two cores for eight elements (Ca, Sr, Cl, Zr, Ti, K, Mn, and Br) and the pollen sums for the four taxonomic groups. The correlation between the two cores were determined based on the coring depth and LOI data. The squared cosine function (Abdi and Williams, 2010) showing the relative weight of influence of a principal component for a given observation was used to estimate the quality of the representation. On the biplot, the first principal component, which shows the largest variation is represented by the Dim1 axis. The second principal component, orthogonal to the Dim1 axis is represented by the Dim2 axis. Categorical variables (bottomland forest, freshwater deltaic lake, intermediate/brackish, saline, and mangrove) were used to distinguish eighty-one individuals. The proximity between a variable and a cluster is positively correlated to correlation, the closer the variable is to a cluster, the higher the correlation. Therefore, longer arrows indicate a larger total variance. Positively correlated variables point in the same direction, while negatively correlated variables point in opposite directions. The closer a variable is to the circle of correlations, the better its representation.

4. Results

4.1. Chronology

The BC64A samples at 53, 116, and 169 cm returned calibrated radiocarbon dates of 106 ± 108, 385 ± 80, and 582 ± 56 yrs BP, respectively. The BC64B samples at 107, 160, 250, and 370 cm gave calibrated dates of 412 ± 88, 581 ± 54, 1277 ± 59, and 3559 ± 78 yrs BP, respectively (SI2). The results were used to develop the age-depth model in Fig. 3. The calibrated dates (from 214 to 0 cm) of both cores were highly correlated as the linear regression model produced a significant linear correlation ($r^2 = 0.986$; $p < 0.01$; n = 213) (SI3).

The ^{137}Cs and ^{210}Pb radiochemistry profiles are displayed in Fig. 4. The first detection of ^{137}Cs was at 27 cm, representing 1954 CE, with the peak of ^{137}Cs occurring at 20 cm, corresponding to 1963 CE. The $^{210}Pb_{xs}$ activity is highly variable throughout the top 40 cm. Sediment accretion rates from the ^{137}Cs and $^{210}Pb_{xs}$ data are 0.36 cm/yr and 0.58 cm/yr, respectively.

4.2. Core stratigraphy

The two cores are highly correlated stratigraphically, consisting of silt/clay from 214 to 160 cm, silt/clay with embedded peats from 160 to 60 cm, interstratified peat/clastic intervals from 60 to 25 cm, and fine sand and clay from 25 to 0 cm BC64B, a 372 cm long core, includes fine sand with embedded peats from 372 to 214 cm.

BC64A is divided into four stratigraphic zones (Fig. 5). Zone 2 (214-160 cm) consists of homogeneous grey silt-clay mixtures, containing 36–61% water content, 5–13% organics, 3–4% carbonates, and 83–91% residuals (mainly silicates). Plant debris (stems and roots) are irregularly embedded throughout the section. Zone 3 (160-60 cm) contains peat/clastic intervals with embedded intact plant debris (stems and roots). The peat intervals at 138-137 cm and 117-112 cm contain up to 30% organics embedded in silt/clay mixtures. The section has 30–75% water content, 1–4% carbonates, and 66–96% residuals. Zone 4 (60-25 cm) consists of fine silt/clay units overlying a peat deposit at 60 cm. Plant stems and roots are present throughout the section. The zone contains 46–61% water content, 5–11% organics, 2–3% carbonates, and 86–94% residuals. Zone 5 (25-0 cm) is mainly comprised of silt/clay mixtures with embedded plant debris (roots and leaves) at the top of the core. Peat/clastic intervals at 25-20 cm contain organic contents up to 11%. This section contains 32–60% water content, 2–3% carbonates, and 85–93% residuals.

BC64B consists of five stratigraphic successions. Zone 1 (372-250 cm) consists of homogeneous sands (101–176 μm) with interbedded organic-rich clay intervals at 350, 327, 315, 285, and 250 cm. The interbedded depositions contain horizontal-planar-lamination with up to 14% organic content. Light-yellow clays are present at 315 and 250 cm; the other clays are dark. Zone 1 contains 21–40% water content, 2–3% carbonates, and 83–98% residuals (Fig. 5). Zone 2 (250-160 cm) is separated from Zone 1 by a sharp contact at 250 cm, clay overlying fine sand, and silt. Zone 2 mainly consists of homogeneous grey silt-clay mixtures with irregularly embedded plant debris (stems and roots). The section contains 24–50% water, 3–15% organics, 1–5% carbonate contents, and 82–95% residuals. Zone 3 (160-60 cm) consists of organic-rich layers and embedded intact plant debris (stems and roots). Peat/clastic intervals (2–5 cm thick) are present between 135 and

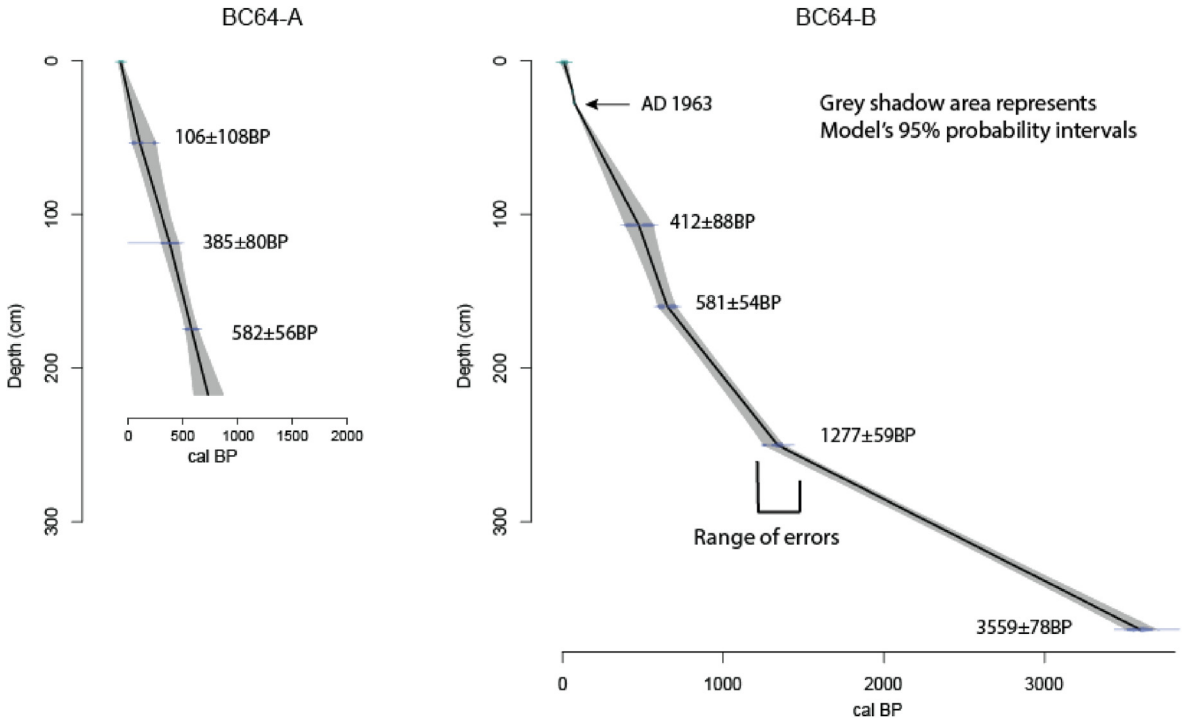

Fig. 3. Age-depth models of cores BC64-A and BC64–B with plotted radiocarbon ages (blue dots). Linear interpolation is made using Clam 2.2 and the R Workspace IntCal 13.14C Northern hemisphere curve (Blaauw, 2010). Grey shadow area represents the model's 95% probability intervals. Length s of blue bars indicate the error ranges.

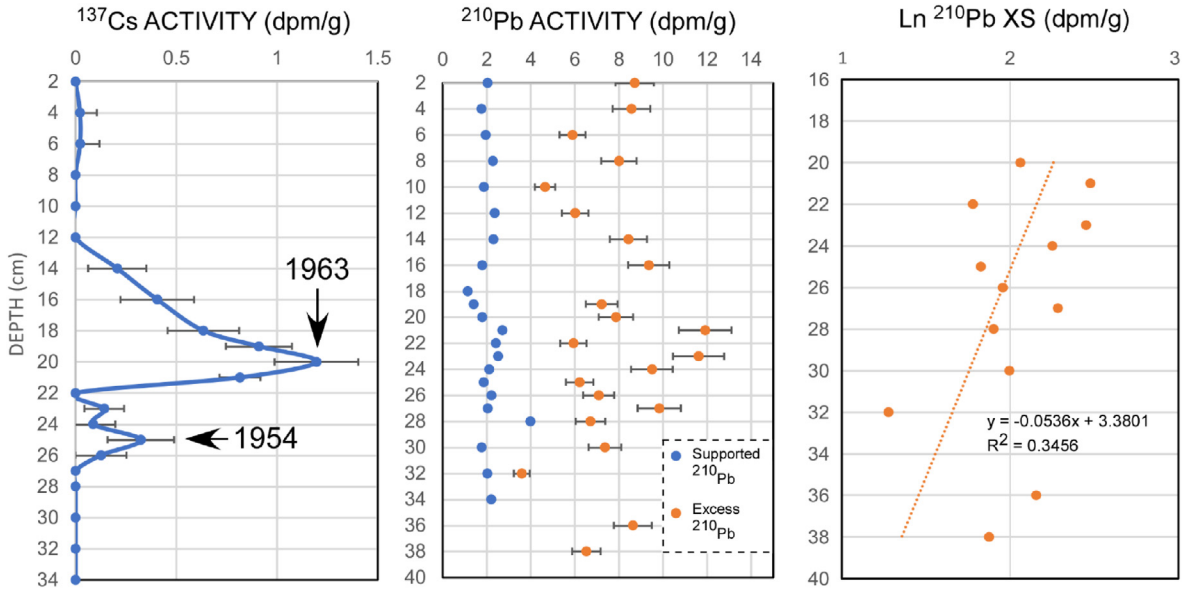

Fig. 4. Radiochemical profiles of BC64B. Summary plots of ^{137}Cs and ^{210}Pb display their activities and geochronology.

124 cm and 110–105 with up to 31% organic contents overlaying clastic sediments. Water content is 27–72%, carbonates are 1–5%, and residuals 63–96%. Zone 4 (60-25 cm) is marked by frequent peat/clastic intervals. Plant stems and roots are embedded in clays, with 39–64% water, 4–13% organic contents, 2–3% carbonates, and 85–95% residuals. Zone 5 (25-0 cm) consists of fine sand to silt and clay. This section contains 45–66% water, 5–12% organics, 2–3% carbonate contents, and 85–93% residuals.

4.3. Granulometry

The grain size distribution analysis indicates various grain size distributions including bimodal, polymodal, trimodal, and unimodal types (SI6, SI7). Sediments were poorly sorted, while a general sedimentary sequence is fining upward with the mean grain size changing from 120.6 to 21.37 μm toward the top of the core (Fig. 5). The bottom section (360-250 cm) generally consists of fine sand and very coarse silt particles from 120.6 to 112.5 μm. Very coarse silt and very fine sand present as light to dark grey while the fine

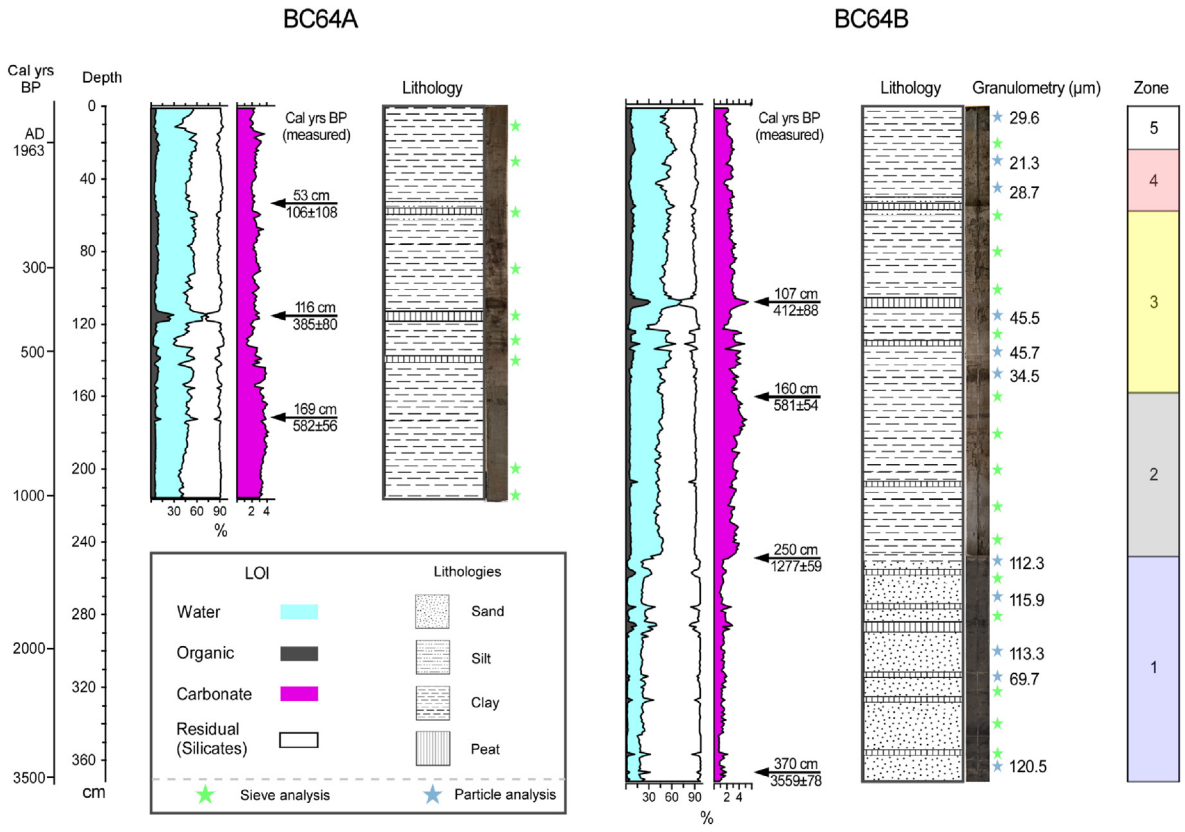

Fig. 5. Loss on ignition (LOI) and granulometry analyses with calibrated radiocarbon dates. LOI curves display percentages of water, organic, and carbonate content. Lithologs show sedimentary characteristics of the five stratigraphic units and granulometry results. Green stars indicate sieved samples, blue stars indicate laser analysis. (For interpretation of the references to color in this figure legend, the reader is referred to the Web version of this article.)

silt to mud is tinted with black (Fig. 5). Unimodal, moderately sorted muddy sand between 360 and 314 cm transitions to moderately sorted sand in 301–270 cm, and to muddy sand at 251 cm. Polymodal, poorly sorted mud at 249 cm transitions to trimodal and bimodal types with poorly sorted sandy mud at 134 cm. The mean grain size in the section ranges from 100.5 to 17.85 μm. Poorly sorted polymodal sandy mud at 116-30 cm displays mean grain sizes from 47.60 to 21.37 μm. The top section at 5 cm consists of bimodal poorly sorted sandy mud with a mean grain size of 29.67 μm (SI6).

4.4. X-ray fluorescence (XRF)

Nine elements (Ca, Sr, Cl, Zr, Ti, K, Mn, Br, and Rb) are presented to characterize geochemical conditions and hydro-environmental changes (Fig. 6). Generally, the XRF profiles of the nine elements are highly correlated across the cores, as terrestrial elemental concentrations are high in zone 1 and 2, with marine elements increasing toward the core top. Clastic particles (fine-sand and silt) correspond to an increase in Zr, Ti and K values while high organic percentages correlate with Br.

Zone 1 shows variations of terrestrial (Zr, Ti, K, Mn) and marine (Ca, Sr, Cl) elements. Episodic spikes of terrestrial elements occur in the peat/clastic intervals, associated with abrupt changes to coarser grains (Fig. 5). Mn concentrations increase in the organic-rich layers between 285 and 250 cm. Cl concentrations increase between 300 and 270 cm, while Ca and Sr values are high throughout the section. Generally, the Zr/Rb ratio increases toward the core-bottom. Zone 2 shows an increase in terrestrial elements (Ti, K, and Mn) although Ca values remain high in both cores. Mn significantly increases in both cores with episodic spikes occurring between 214 and 160 cm. In general, silt particles correspond to an increase in Ti and K values. Cl/Br ratio is low throughout the section. Zone 3 displays a gradual increase in Br concentrations. Ca and Sr values are generally low or undetectable, while Cl gradually increases toward the core-top in both cores. The fluctuations in Sr and Cl values are negatively correlated with water, organics, and carbonates values, while the episodic spikes of the Zr/Rb ratio are negatively correlated with water and organic percentages. Zone 4 shows generally high Br concentrations associated with intervals that contain >10% organics. Episodic spikes of Zr, Ti, and K are negatively correlated with Cl concentrations. Sr is positively correlated with the Zr/Rb ratio. Zone 5 displays significant gradual increases in marine elements (Cl, Ca, and Sr). Episodic spikes of K and Ti are positively correlated with low water and organic percentages.

4.5. Pollen assemblages

A total of 62 pollen and spore (*Pteridium* and Polypodiaceae) taxa, as well as foraminifera (Ammonia) test, were detected and counted to identify ecological shifts (Fig. 7). The maximum percentages of major taxa are presented. Zone 1 (372-250 cm) is represented by high percentages of *Taxodium* (up to 72%) and other arboreal pollen taxa, including *Quercus* (>40%), Betulaceae (*Alnus*, *Betula*, and *Carpinus* up to 15%), *Pinus* (>35%), *Salix* (>25%), Rhamnaceae (>14%), *Myrica* (>12%), and small percentages of *Juglans*, *Carya*, *Ulmus*, *Celtis*, *Rhus*, Oleaceae, *Platanus*, *Liquidambar*, *Populus*, Rosaceae, *Acer*, *Fraxinus*, *Cornus*, *Sapium*, *Cephalanthus*, and Vitaceae. Non-arboreal pollen taxa include Cyperaceae (>15%), Poaceae

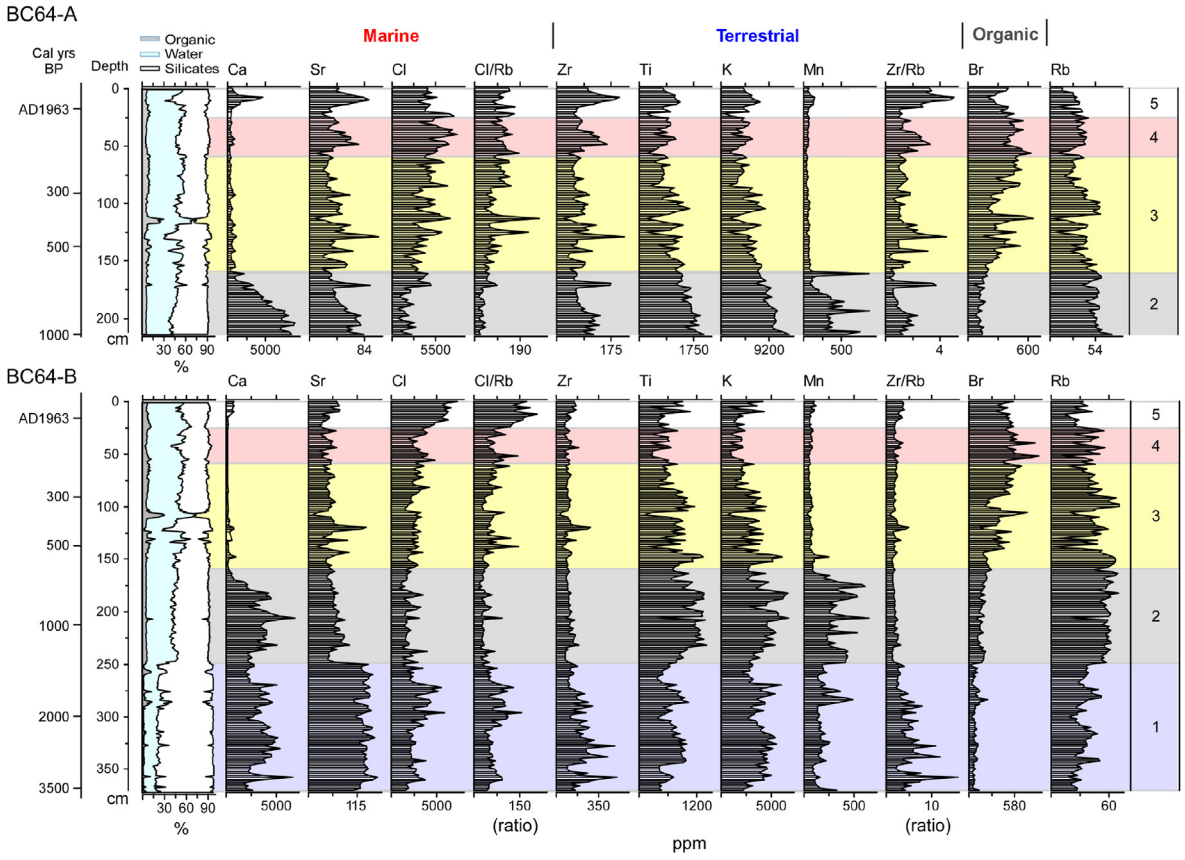

Fig. 6. LOI and XRF analyses of BC64A and BC64B with calibrated radiocarbon dates. Profiles of marine (Ca, Sr, and Cl), terrestrial (Zr, Ti, K, and Mn), and organic (Br) indicators are displayed.

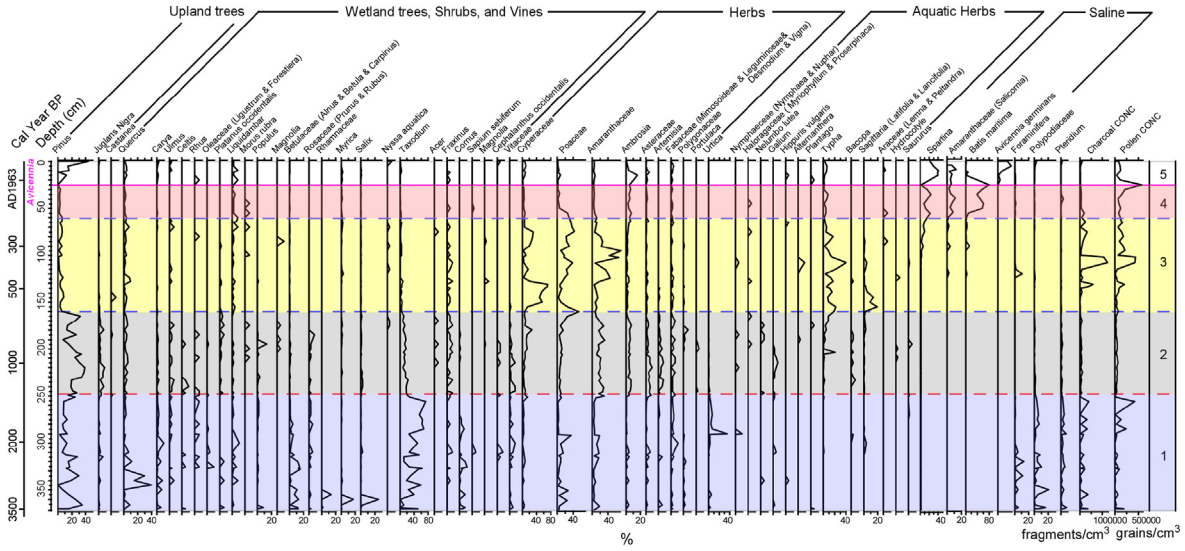

Fig. 7. Pollen diagram of BC64B with calibrated radiocarbon dates. 62 pollen taxa and spores representing >1% of the sum are shown. Pollen and charcoal concentrations are graphed as grains per cubic centimeter and fragments per cubic centimeter, respectively.

(>35%), Urticaceae (>35%), and Amaranthaceae (>15%), and small percentages of *Ambrosia*, Asteraceae, *Artemisia*, Fabaceae, and Polygonaceae. Small percentages of such tidal freshwater herbs as *Sagittaria* (<2.5%), *Typha* (>1%), Nymphaeaceae, *Nelumbo*, *Galium*, *Hippuris*, *Plantago*, *Bacopa*, Araceae, and *Saururus* are present. Two spore taxa, Polypodiaceae and *Pteridium* are abundant around 320 cm. Foraminifera (*Ammonia*) tests are abundant between 372 and 330 cm.

Zone 2 (250-160 cm) shows a low pollen concentration and high percentages of upland taxa such as *Pinus* (>38%) and *Juglans nigra* (>4%). Generally, arboreal pollen taxa decrease toward the top, namely *Taxodium* (>23%), *Quercus* (>5%), *Carya* (>1%), *Ulmus* (1%),

Rhus (<1%), *Platanus* (<2%), *Populus* (>13%), *Betula* (<2%), Rosaceae (>1%), *Myrica* (>1%), *Salix* (<3%), *Fraxinus* (>1%), and Vitaceae (<3%). Increasing non-arboreal taxa include Cyperaceae (>27%), Poaceae (>25%), Amaranthaceae (>28%), *Ambrosia* (>7%), Asteraceae (>7%), *Artemisia* (<2%), Fabaceae (<2%), Polygonaceae (<3%), and Urticaceae (>3%). Tidal freshwater herbs consist of *Typha* (>18%), *Bacopa* (1%), *Sagittaria* (2%), *Galium* (>1%), and *Saururus* (<2%), and small percentages of Nymphaeaceae, Haloragaceae, *Nelumbo, Alternanthera, Plantago, and Hydrocotyle*.

Zone 3 (160-60 cm) is represented by high pollen and charcoal concentrations. *Typha* (>35%), *Sagittaria* (>14%), Cyperaceae (>70%), Poaceae (>61%), and Amaranthaceae (<70%) are the most abundant pollen types. Small percentages of herbaceous taxa are present, including *Ambrosia* (>6%), Asteraceae (>3%), Fabaceae, Nymphaeaceae, Haloragaceae, *Hippuris*, *Alternanthera*, *Bacopa*, Araceae, *Hydrocotyle*, and *Saururus*. Pollen and charcoal concentrations are highly variable between 133 and 80 cm, positively correlated with the fluctuations in tidal freshwater herbs. Between 120 and 115 cm, small percentages of *Spartina* (>6%) and *Batis* (>14%) occur along with foraminifera (*Ammonia*) tests. The peaks of charcoal and pollen concentrations marked between 108 and 102 cm. Main arboreal taxa include *Quercus* (<10%), *Liquidambar* (2%), *Populus* (>1%), *Magnolia* (<3%), *Myrica* (>2%), *Taxodium* (<9%), and *Fraxinus* (>1%). Small percentages of *Carya*, *Ulmus*, *Celtis*, *Rhus*, *Platanus*, *Morus*, Betulaceae, *Salix*, *Nyssa*, *Acer*, Vitaceae, *Juglans*, and *Pinus* are present.

Zone 4 (60-25 cm) is represented by a sharp increase in such salt marsh taxa such as *Spartina* (>18%), *Batis* (>66%), and *Salicornia* (>11%). Only small percentages of arboreal taxa such as *Pinus* (>6%), *Quercus* (>3%), *Liquidambar* (>2%), *Myrica* (>1%), and *Taxodium* (>2%) are present. Other non-arboreal pollen taxa include Cyperaceae (>7%), Poaceae (>47%), Amaranthaceae (>5%), *Ambrosia* (>7%), Asteraceae (>1%), and *Typha* (>7%).

Zone 5 (25-0 cm). *Avicennia* pollen first occurs at 25 cm and increases in percentage up to 9.4% toward the top, inversely proportional to *Spartina* percentages. Arboreal pollen taxa include *Pinus* (>44%), *Quercus* (>4%), *Carya*, and *Myrica*. Saltmarsh plants including *Spartina* (32%), *Batis* (87%), *Salicornia* (>12%), and Cyperaceae (>10%), dominate the herbal taxa. Other non-arboreal taxa are *Ambrosia* (>16%), Asteraceae (4%), Poaceae, Amaranthaceae, Fabaceae, *Hippuris*, *Plantago*, *Typha*, and Araceae. Small percentages of foraminifera (*Ammonia*) tests are present between 15 and 25 cm.

4.6. Statistical analysis

The PCA-biplot displays ecosystem clusters and distance matrices for four taxonomic groups and chemical elements (Fig. 8). The first principal component (the Dim1 axis) accounts for 44% of the total variance, with the second principal component (the Dim2 axis) accounting for 25.2% of the variance. Terrestrial elements (Ti, K, and Mn) are positively correlated on both the Dim1 and 2 axes, having high positive loadings for both. Marine elements (Ca, Sr) display positive loadings on the Dim1 axis, while Cl has negative loading on both Dim1 and 2 axes. Bottomland forest variables clustered in the fourth quadrant are highly correlated with floodplain trees, terrestrial (Zr), and marine (Sr) elements. Ca, which accounts for 88% of the variability of the Dim1 axis, is moderately

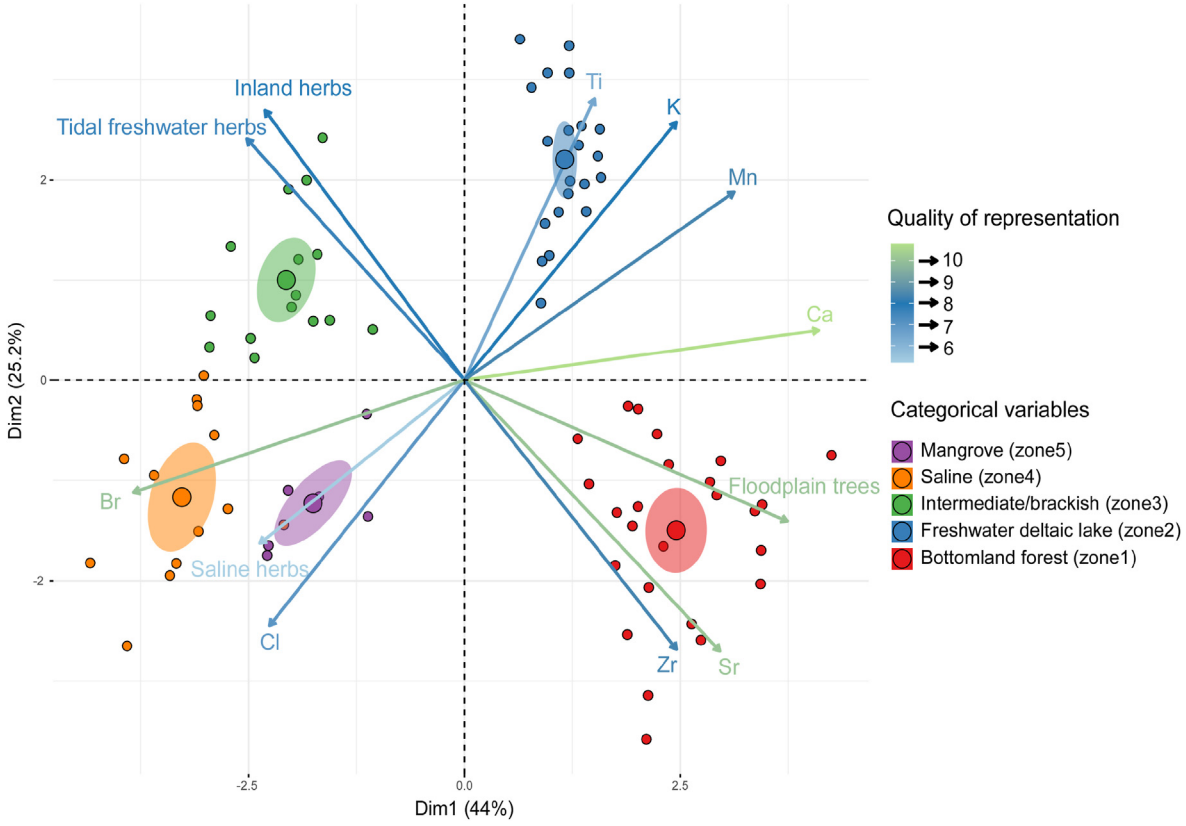

Fig. 8. The PCA-biplot elucidates the correlation between terrestrial and marine sedimentary sources and the existent ecosystems type. The biplot displays ecosystem clusters (bottomland forest, freshwater deltaic-lake, intermediate/brackish marsh, saline and mangrove) and distance matrices for taxonomic groups and chemical elements. The first Principal Component (the Dim1 axis) accounts for 44% of total variance, with the second Principal Component (the Dim2 axis) accounting for 25.2% of total variance. Longer arrows indicate larger total variance. Bigger dots indicate centers of the variables.

correlated with bottomland forest variables. Freshwater deltaic-lake variables clustered in the first quadrant highly correlate with the terrestrial elements. Intermediate/brackish variables clustered in the second quadrant are highly correlated with tidal freshwater herbs and inland herbs. Br, accounting for 87% of the variability of the Dim1 axis, has a high negative loading and is associated with mangrove and saline variables. Saline and mangrove variables clustered in the third quadrant are highly correlated with saline herbs and moderately correlated with Cl. Terrestrial elements (Ti, Mn, and K) are negatively correlated with saline herb and Cl.

5. Discussion

5.1. Geochronological variability

An extremely dynamic deltaic environment results in broad-scale geomorphic changes and significant geological variabilities in the Mississippi River delta complex. Channelization, crevasses, or overbank splays depositing various minerals and organic materials result in wide variability in grain size and radiocarbon dates (Flocks et al., 2006). In addition, different dating techniques (e.g., optically stimulated luminescence (OSL) versus radiocarbon dating techniques; Briant and Bateman, 2009) have possibly added to the uncertainty to the dating of the active periods of St. Bernard and Lafourche delta complexes. To minimize the geological variability, we have defined the active period of the Mississippi delta complexes according to the chronologies based on the radiocarbon chronologies (Frazier, 1967; Levin, 1990; Kindinger et al., 2001; Rodrigues et al., 2021: SI4). BC64A and B highly correlate with St. Bernard (lobe7-Bayou des Families: dark purple) and Lafourche (lobe10-Bayou Blue: dark orange) delta complexes indicating the possible ranges for extended deltaic plains (Fig. 9). The St. Bernard delta complex extended its multiple distributaries to the southeast of the study site between 3600 and 2600 BP (Frazier, 1967; Levin, 1991; Flocks et al., 2006). The Lafourche delta complex (e.g., Bayou Blue delta) fully developed between ~2600–1900 BP (Frazier, 1967; Kosters et al., 1987; Levin, 1991). Bayou Blue was a secondary Lafourche Delta, a major distributary channel that prograded eastward over the drowned distal margin of St. Bernard delta complex where it formed Grand Isle (Levin, 1990; Flocks et al., 2006). Levin (1991) suggests that the Lafourche delta progradation continued until ~1900 BP, after which Blue Bayou was almost entirely abandoned, experiencing delta subsidence, with peat accumulating at the site until the development of the Bayou Lafourche delta ~700 years BP (Penland et al., 1988; Day et al., 2007; Chamberlain et al., 2018). The Bayou Lafourche delta prograded through several distributaries and eventually developed a large portion of the present delta plain in the Port Fourchon area. In 1904 Bayou Lafourche was artificially dammed upstream (Kolb and Van Lopik, 1966; Levin, 1991).

5.2. Paleo-environmental reconstruction

5.2.1. Zone 1 (4000–1300 BP) interdistributary swamp and marsh

After 4000 BP, the predominant cross-bedded organic-rich silt and fine sand and high *Taxodium* pollen percentages (>50%) indicate an interdistributary *Taxodium* swamp formed on the distal portion of the St. Bernard inland delta plain, which formed around 3500 BP. The interbedded organic silt and mud and the occurrence of the terrestrial indicators, Ti, K, Zr suggests that fluvial processes such as overbank muds and crevasse splays filled the space between interdistributary and distributary networks (Fig. 10 stages 2–3). The high Zr/Rb ratio and terrestrial values associated with homogeneous fine sand suggest intense delta progradation (Ryu et al., 2021a). Zr correlated with floodplain trees in the fourth quadrant of the PCA biplot suggests that fluvial process likely proliferated in the bottomland swamp ecosystem. The muds deposited during 3500–2000 BP likely resulted from the St. Bernard delta progradation, which developed an extensive deltaic plain during this period (Frazier, 1967; Levin, 1991, Fig. 3).

Periodic sheet-flows of sediment-laden waters over the interdistributary wetlands, the principal means of sediment supply to deltaic plains, likely occurred during this time. High Ca and Sr concentrations may be associated with the redistribution of biogenous sediments deposited in the interdistributary bay prior to initiating river deltas. Coastal areas remained dominated by biogenous and lithogenous sediments (Webb, 2019), while small fragments of foraminifera and shell are buried by terrestrial sediments during the early stage of delta progradation. River beds scoured by massive river discharge downmixed sediments in the new path, building a new delta in a new location (Elliott, 1986).

Pollen assemblages reflecting the local-to regional vegetation communities suggest that isolated cypress (*Taxodium*) swamps along with other bottomland trees, namely *Nyssa*, *Salix*, *Myrica*, and *Fraxinus,* and freshwater marsh plants such as *Sagittaria*, Nymphaeaceae, and *Hippuris* developed in the interdistributary depression during the maximum delta development ~2000 BP. Woody plants and herbs seem to have colonized abandoned interdistributary channels with the subsequent creation of oxbows maintaining the swamps (Shankman and Drake, 1990). Abundant arboreal pollen taxa suggest that hardwood trees such as hickory (*Carya*), wax myrtle (*Myrica*), oak (*Quercus*), and dogwood (*Cornus*) occurred in such areas of higher elevation as natural levees (Fig. 11).

5.2.2. Zone 2 (1300–700 BP) freshwater deltaic-lake

Around 1300 BP, the water level deepened at the site after the Bayou Blue delta was abandoned and lakes formed in the lower sections of the delta plain, as marked by the sharp contact at 250 cm. The clay overlying fine sand-silt likely resulted from channel migration causing overbank flows depositing fine sand to clay as indicated by abundant terrestrial plant pollen percentages. Coastal lakes can originate through the destruction of former swamp and marsh areas as bank erosion occurs along streams, and/or the exhumation of swamp and marsh deposits. Elevated Mn concentrations imply a relatively deep water condition as Mn is reductively dissolved by the action of bacteria living within pond sediments (Donahoe et al., 1994), thereby enriching Mn concentrations in deeper water (Schaller and Wehrli, 1996). The lake phase lasted until ~600 BP. The horizontal laminations within the homogeneous sediment that occur throughout the zone indicate near-continuous subaqueous deposition (i.e., a lacustrine environment). Elevated metal elements (Ti, K) correlated with freshwater deltaic-lake variables in the first quadrant suggest terrestrial sediment input. These metals [Zr, Ti], mainly derived from igneous rocks, not locally present (Dill, 2010), imply that local subsidence resulted in terrestrial sediment input from fluvial discharge into the lake while the delta-lobe building remained the dominant physical process. The swamps located in the inland-most portion of palustrine wetlands were degraded rapidly as a result of limited streamflow associated with the delta-lobe switching and the subsequent abandonment of their main channels (Saucier, 1994; Törnqvist et al., 2008). The high concentrations of Polypodiaceae and *Pteridium* indicate a considerable deposition through water transport (Chmura, 1990; Crowley et al., 1994) evidencing unstable hydrologic status. High calcium concentrations are observed, while strontium concentrations are low. This inverse ratio is unusual in a coastal environment. This anomalous relationship between marine indicators likely results from relic calcareous sediments as iron-bearing calcite ($(Ca, Fe)CO_3$) (Nriagu and Dell, 1974; Dill, 2010). This suggests uneven topography, with expanded lakes and

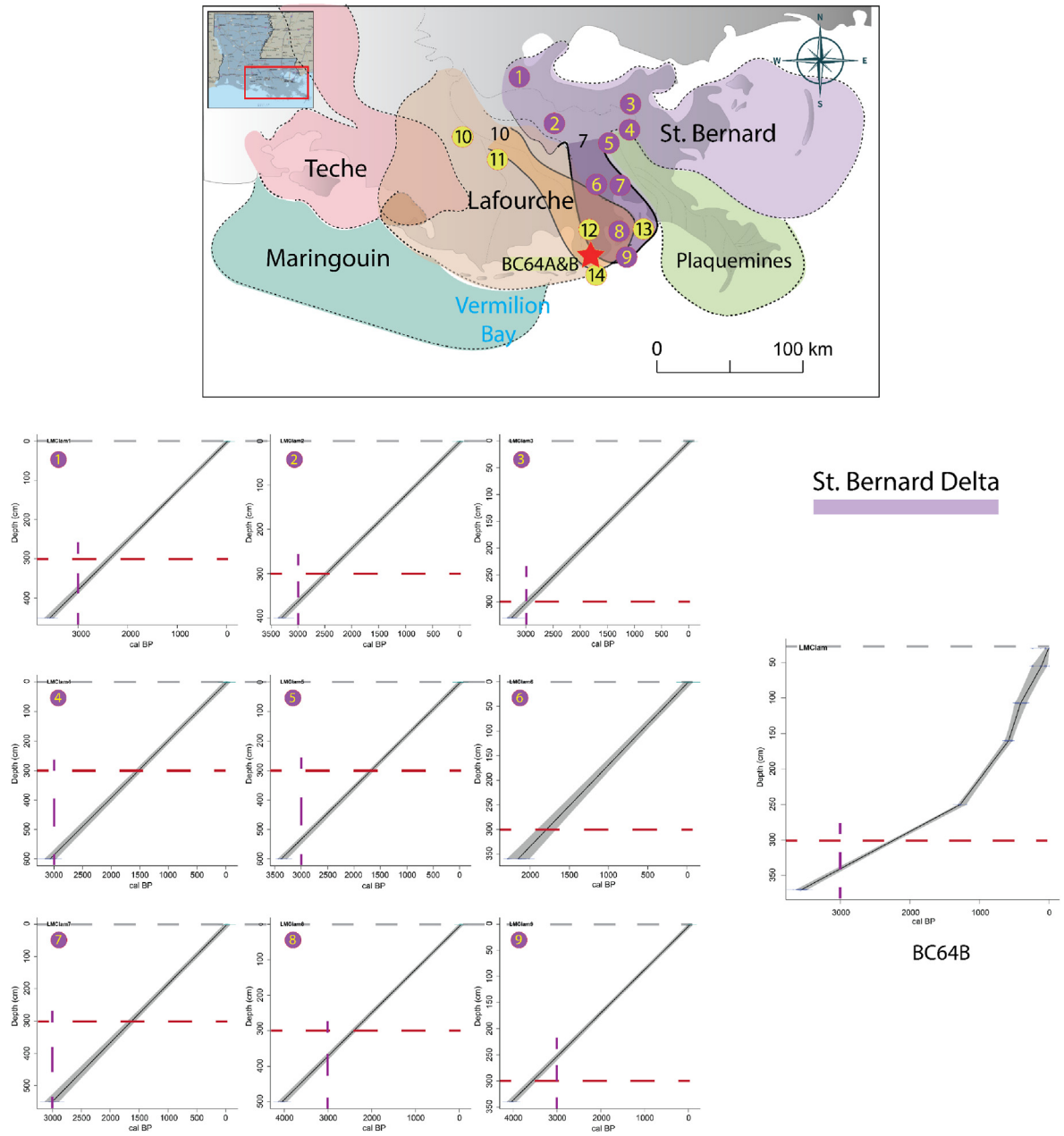

Fig. 9. Fig. 9.1. The St. Bernard (lobe7-Bayou des Families: dark purple) and Lafourche (lobe10-Bayou Blue: dark orange) delta complexes indicate the possible ranges for extended deltaic plains. The purple (lobe 7) and yellow (lobe 10) circled numbers mark the coring sites and their latitude, longitude, with calibrated carbon dates with depths are displayed in SI4. The calibrated carbon dates were applied to age-depth model to compare geochronological cross-correlations with respect to BC64B core showing high correlations with core numbers 1, 2, 3, 8, and 9, and low correlations with 4,5,6, and 7. The grey-dashed line marks 0 cm. The red (x-axis) and purple dashed (y-axis) lines indicate 300 cm depth of core and 3000 cal BP, respectively. Fig. 9.2. Calibrated carbon dates from the Lafourche delta complex applied to age-depth model, in order to compare geochronological cross-correlations. BC64B displays high correlations with cores 11, 13, and 14 and low correlations with cores 10 and 12. The grey-dashed line marks 0 cm. The blue (x-axis) and orange dashed (y-axis) lines indicate the 150 cm depth of BC64B and 1000 cal BP, respectively. . (For interpretation of the references to color in this figure legend, the reader is referred to the Web version of this article.)

wetlands, surrounded by higher ridges, reflecting the uneven subsidence of the delta lobe as a result of delta-lobe switching. Pollen percentages mark an increase in such upland trees as *Pinus*, *Juglans*, and herbaceous plants such as *Ambrosia*, Asteraceae, *Artemisia*, and Fabaceae, matched by a significant decrease in *Taxodium*. The abundance of woody plants and herbs (*Typha*, *Bacopa, Sagittaria*) indicates a freshwater environment. The abandonment of the delta lobes resulted in limited sediment supply and land subsidence, leading to uneven topography with spatially variable ecosystems (Fig. 11: D, E).

5.2.3. Zone 3 (700-200 BP) intermediate and brackish marsh developments

Beginning ~700 BP, the progradation of the Bayou Lafourche delta onto the site (Chamberlain et al., 2018) accelerated the encroachment of intermediate marshes, as indicated by the replacement of emergent aquatic plants such as *Sagittaria*, typically growing in swamps or lakes by Cyperaceae and Poaceae. Fluvial

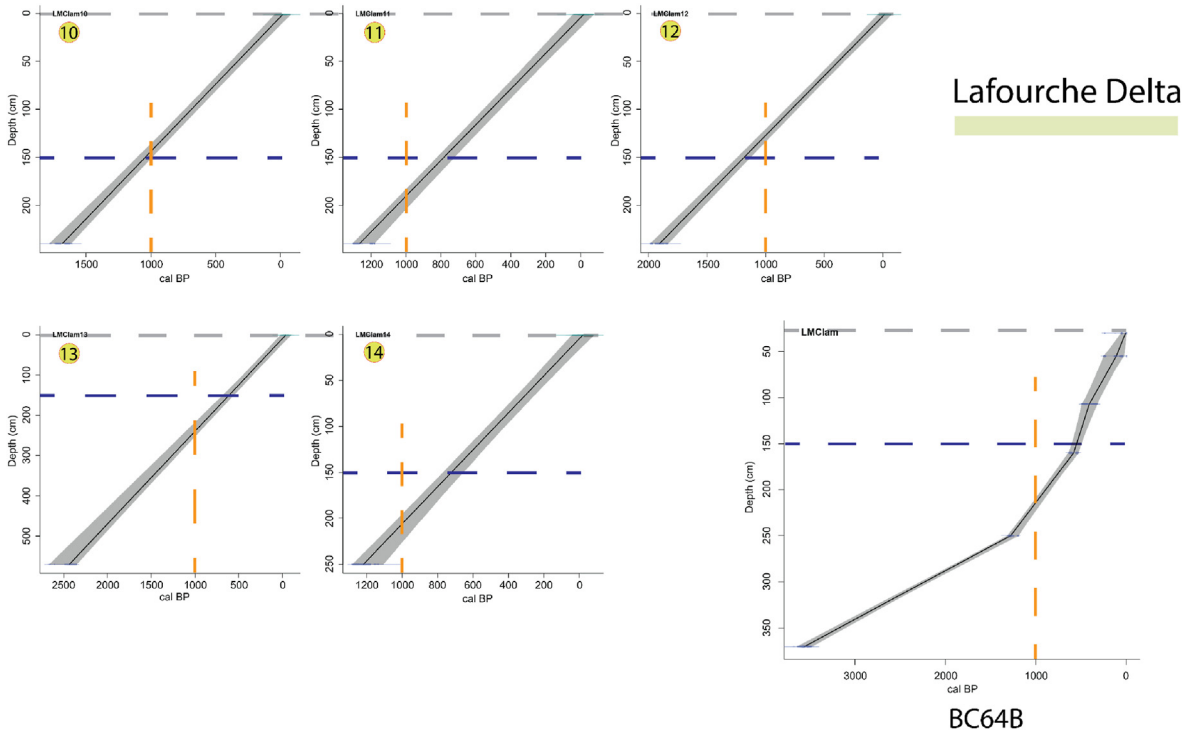

Fig. 9. (*continued*).

sediment delivered from the river facilitated marsh accretion, as indicated by elevated levels of terrestrial elements (Fe, K, and Br) and correlations of tidal freshwater herbs with intermediate marsh variables. As peat accumulated the emergent aquatic plants were generally replaced by *Typha*, Poaceae, and Amaranthaceae ~400 BP. A significant reduction of Ca and stable values for the terrestrial elements Ti, K suggests a continuous terrestrial sediment input. Elevated Br concentrations indicative of high organic content suggest a relatively stable marsh condition until 300 BP. Afterward, ~200 BP peat/clastic intervals containing foraminifera (*Ammonia*) tests and the replacement of *Typha* by Poaceae (mainly *Spartina*), *Salicornia*, and *Batis* with elevated Cl concentrations suggest a brackish marsh environment and repeated marine incursions, likely associated with hurricane-generated storm surges, resulting from the coastal retreat associated with the abandonment of the Bayou Lafourche delta (Gerdes, 1982; Penland et al., 1988).

High charcoal concentrations following the organic peak suggest larger/more intense fire, resulting from heightened fuel loads associated with tropical cyclone damage (Hutley et al., 2013). The combined effects of storm surge, wind damage to the arboreal component, and limited sediment supply were likely the main drivers of the ecological shift from intermediate marsh to salt marsh. Saltmarsh plant communities dominated by Poaceae (mainly *Spartina*) and *Batis* began to increase in the areas as the vulnerability of the fresh/brackish ecosystems increased.

5.2.4. Zone 4 (200BP-AD, 1900s) saltmarsh

As the Mississippi River began discharging into the Plaquemines-Balize deltas during the last few centuries, the Bayou Lafourche delta plain subsided due to reduced supplies of fresh water and sediment, as marked by abundant plant stems and roots. Saline variables, correlated with Cl and saline herbs in the third quadrant of the PCA biplot, and the increase in marine elements (Ca and Sr) indicate increasing marine influence. Pollen data, (the expansion of the saltmarsh plants such as *Spartina*, *Batis*, and *Salicornia*), in conjunction with elevated Br concentrations, indicates that plant debris was the major sedimentary source. Minimal sedimentary changes between zones 3 and 4 indicate that the transition from intermediate to saltmarsh was gradual.

During the 19th century, the Caminada-Moreau Headland eroded at a rate of >18 m/yr (Morgan and Larimore, 1957; Penland et al., 2005; Dietz et al., 2018) (Fig. 1C). Clastic sediments deposited since 1800 CE may be associated with increasing storm surge overwash as the site's proximity to the sea increased dramatically. Peat/clastic layers with embedded foraminifera (*Ammonia*) occur in this zone, almost undoubtedly the result of storm surges.

5.2.5. Zone 5 (1900s CE -present) mangrove swamp

Avicennia germinans pollen first occurs at 25 cm, dating the first appearance of black mangrove at our study site to the early 20th century. The increase in black mangrove percentage [up to 9.4%], inversely proportional to *Spartina* percentages toward the top of the core, suggests that the expansion of mangroves into existing *Spartina* marshes has occurred somewhat episodically in the coastal wetlands of Louisiana (O'Neil, 1949; Sherrod and McMillan, 1985; Perry and Mendelssohn, 2009; Osland et al., 2017). Previous studies document the presence of black mangroves in salt marshes adjacent to Bayou Lafourche up to Leeville (O'Neil, 1949; Perry and Mendelssohn, 2009) and in the nearby Vermilion Bay (Sherrod and McMillan, 1985) (Figs. 1 and 2). Elevated concentrations of the marine indicators (Cl and Ca) indicate that the site has become increasingly saline since the 1800s. Larger grain size associated with high Cl/Br ratio in clastic layers and high carbonate contents suggests high-energy marine incursions. Coastal Louisiana is frequently struck by tropical cyclones. Historical documents recorded the occurrence of hurricanes within 100 km of our site in 1901 (Unnamed-Grand Isle), 1915 (Unnamed-New Orleans), 1947 (Fort Lauderdale-Grand Isle), and 1956 (Hurricane Flossy-Grand Isle) (Roth, 2010: SI5). The distinct peat/clastic intervals above 67 cm are concordant with early 1901–1902 which are, in turn,

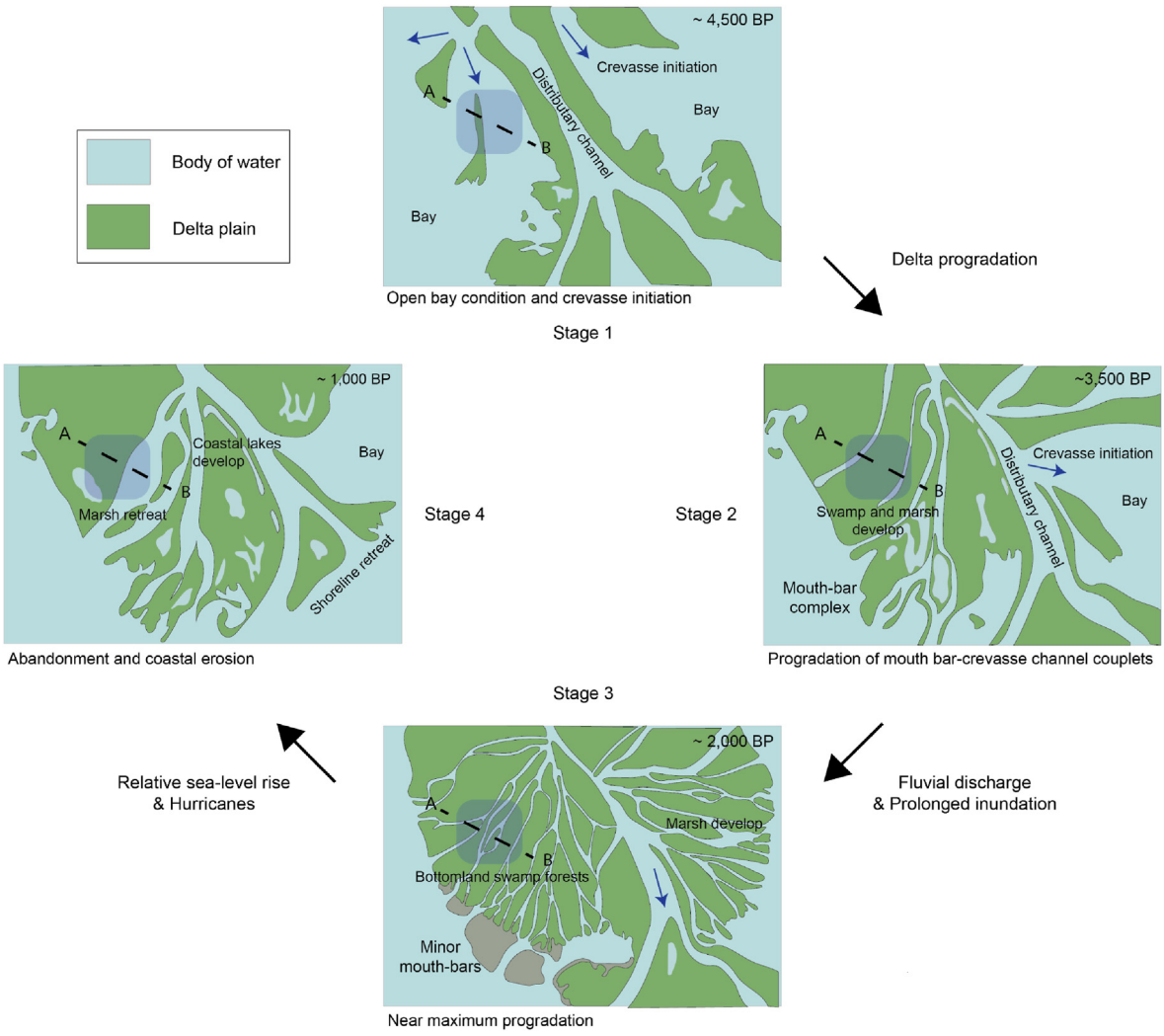

Fig. 10. Schematic representation of the evolution of the interdistributary/distributary system. Our study site is in a dark-blue square between the line (A–B) shown in Fig. 11. After the initiation of delta progradation, abundant sediment and water supplies from the distributary channel filled the interdistributary bays in stage 1. In stage 2 crevasse splays fill the lower ground with sediment, and swamp and marsh ecosystems develop on the higher ground. In stage 3 near-maximum progradation and abundant fluvial discharge lead to the formation of dense bottomland hardwood forests over the delta plain. In stage 4 delta abandonment and relative sea-level rise causes marsh and shoreline retreats while the delta plain transitions to coastal lakes or open water. (For interpretation of the references to color in this figure legend, the reader is referred to the Web version of this article.)

consistent with the early historical hurricane records.

5.3. Climate variability and mangrove establishment

Kiage (2019) found an early establishment of *Rhizophora* shortly after cal 1450 CE and 1640 in the vicinity of Bay Jimmy (Fig. 1B) during the early part of Little Ice Age (LIA), which was characterized by cold and dry conditions in Louisiana. However, our study does not identify *Rhizophora* pollen at our study site during this time and does not support the scenario of red mangrove being present at the site during the LIA. A possible contributing factor for the absence of mangroves at our site during the past millennium was the prograding Plaquemines-Modern delta lobes that delivered large volumes of freshwater and fluvial sediment to the area (Roberts, 1997; Bomer et al., 2019), thereby decreasing the salinity and allowing freshwater communities to outcompete mangroves. Although, mangroves have arrived at the Louisiana coast in the 1700s (Osland et al., 2020b), our pollen record only documents the establishment of *Avicennia* during the past century, with a rapid expansion occurring over the most recent decades. The occurrence of warmer winters, coupled with anthropogenic activities (dredging canal), may have facilitated the recent expansion of *Avicennia*. Powerful hurricanes may have driven the spread of mangroves by transporting their propagules farther inland and dispersing them widely along the Gulf Coast (Jiang et al., 2014).

Paleoenvironmental reconstruction summary; A sequence of five major ecosystems occurred at our study site since 3500 BP:

1) a *Taxodium-Nyssa* freshwater forest and marsh (4.0–1.3 cal yr BP),
2) a *Typha-Bacopa* freshwater deltaic-lake (1.3–0.7 cal yr BP)
3) an intermediate and brackish marsh developments (0.7–0.2 cal yr BP),
4) a *Spartina*-dominated saline marsh (0.2 cal yr BP - ~1950 AD),
5) a short stature A. *germinans* forest (1950-present).

5.4. PCA as a means of inferring drivers

Naturally, each of the five environments in this sequence

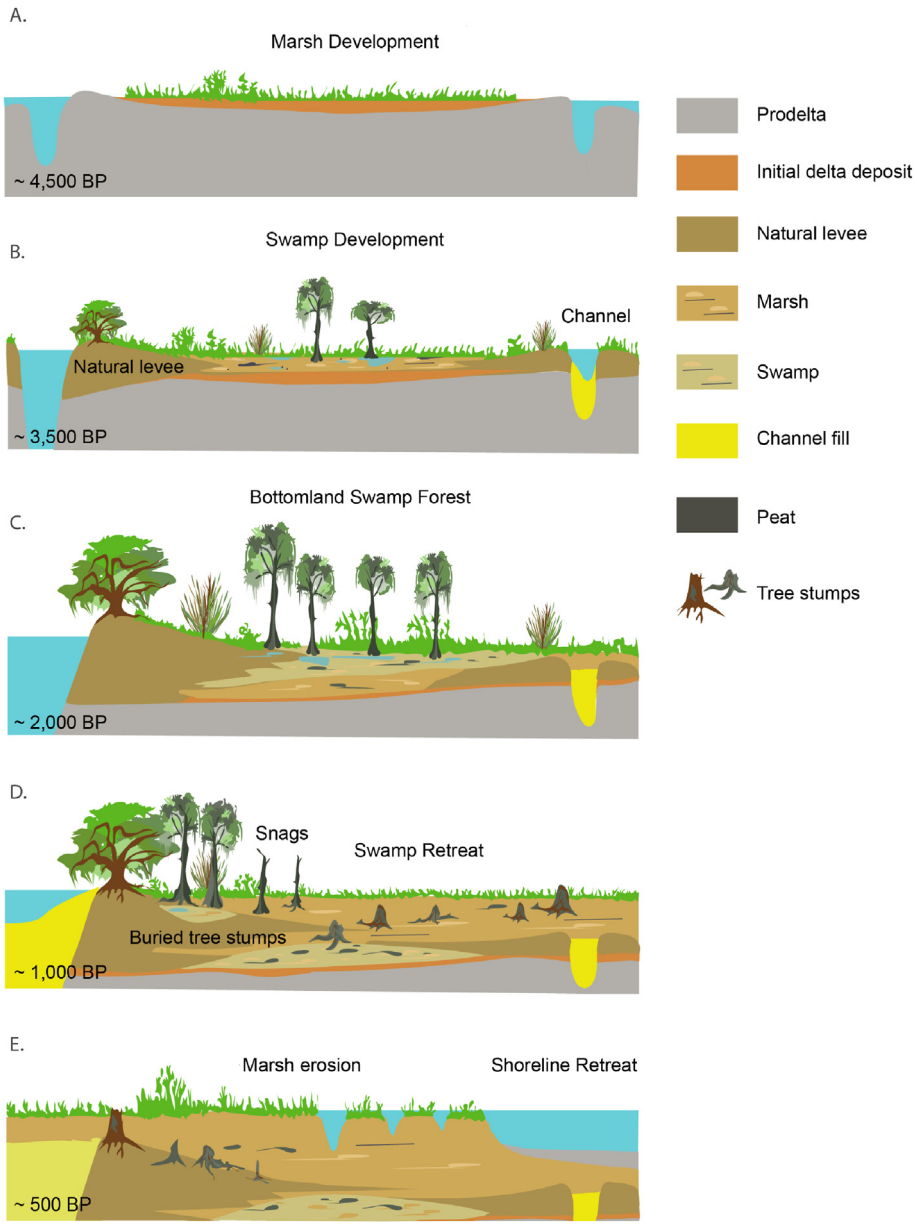

Fig. 11. Hypothesized model of wetland evolution on a delta plain. A: Initial delta develops under strong fluvial discharge. Tidal freshwater herbs establish in lower ground and woody plants occur on relatively higher ground (e.g., levee). B: Extensive marsh and initial swamp communities ensue due to abundant sediment-rich freshwater input from multiple channel developments. C: Diverse swamp forest and marsh ecosystem, with various geomorphological change (e.g., levee and meander cutoff) likely contributes to the nourishment of swamp ecosystems. D: Reduced sediment and freshwater supplies cause swamp retreat. E: Marsh erosion due to reduced sediment and relative sea-level rise. Increased biomass associated with the formation of hydrogeomorphic landforms.

developed as a response to the ambient environment, with zone changes corresponding to altered background parameters. A specific objective of this study is to identify the external forcing agent(s) driving each change, as a means of better understanding the processes controlling the ecological dynamics of the Louisiana coast, with the possibility of applying this knowledge to current and future conditions. To achieve this aim, we have applied PCA as a means of identifying correlations between the geochemical and ecological variables. By correlating specific ecosystem types to specific geochemical signatures, we can hypothesize the source of sedimentary material, and reverse engineer that information into identifying the probable proximate cause of the environmental change.

The PCA-biplot provides several examples of the correlation between terrestrial/marine sedimentary sources and the existent ecosystem type (Fig. 8). The correlation between freshwater deltaic-lake variables and the metals Ti, Mn, and K suggest that terrestrial sediments are strongly associated with lacustrine environments. Because Br is indicative of organic sediments (Ryu et al., 2018), the association of high negative loading of Br with saline and mangrove variables implies that organic sedimentary sources are important components of saline and mangrove environments. The strong negative correlations between terrestrial elements Ti, Mn, and K and Cl suggest that these four elements can be used to distinguish fluvial and marine influences. The bottomland forest variable is correlated with both terrestrial (Zr) and marine (Sr and Ca) elements, implying that terrestrial material is likely strongly associated with floodplain trees, while marine materials are greatly

influenced by sediment redistribution (e.g., relic calcareous sediments) and sediment reworking during land subsidence. Saline herbs and Cl highly correlated with mangrove and saline variables indicate that both ecosystems share the same environment and that marine impacts such as storm surge and saline water incursion greatly contribute to establishing a saline environment. The association between Br and tidal freshwater herbs, inland herbs, and saline herbs suggests that organic-rich sedimentary sources are likely important to fresh/intermediate and saline environments. Based on Fig. 8 PCA-biplot, we infer that fluvial-lacustrine processes deliver large quantities of terrestrial materials, which are significant contributors to freshwater deltaic-lake and bottomland forest ecosystems, while saline and mangrove environments are heavily affected by marine impacts.

5.5. Inferred drivers

Using the PCA-based correlations as a means of identifying probable water and sediment sources for each zone, we can identify likely forcing agents. Fig. 8 shows a clear, unidirectional movement from fresh (bottomland forest, zone 1) to saline (Mangrove, Zone 5), with each zone displaying distinct chemical and ecological signatures. The differences in ambient background parameters between zones are marked by the associated PCA variables. The transition from bottomland forest to freshwater deltaic lake (zone 1–2) is marked by an increase in Mn, K, and especially Ti, terrestrial indicators suggesting an increased influence of fluvial material (material derived from nonlocal sources), corresponding to delta progradation.

The shift from freshwater deltaic lake to intermediate brackish (zone 2–3) corresponds to the increasing influence of inland herbs, tidal freshwater herbs, and Br concentrations, likely associated with lobe abandonment, subsidence, and the subsequent increase of marine influence.

The shift from intermediate/brackish to saline (zone 3–4) is marked by increasing Cl and saline herbs, indicating increasing salinity/marine influence, likely associated with coastal retreat and RSLR. The transition from saline to mangrove (zone 4–5) is a continuation of this process.

The PCA biplot (Fig. 8) makes clear that the terrestrial and marine elements are clearly differentiated by their environmental signatures, especially the inverse relationship between Br and Ti, K, with a unidirectional movement (counterclockwise on the biplot) from fresh to saline over time as salinity increases. However, it is important to note that the unidirectional salinity increase is not driven by a single external forcing agent, rather each shift results from a particular driver(s), the relative influence of which changes over time.

In the early part of our record, the main driver of these ecological shifts was clearly the delta cycle. The site's early ecological history displays the standard delta cycle successions. First, an open bay in an interdistributary location ~4500 BP (Fig. 10: Stage 1). Then, between 3500 and 2000 BP as the St. Bernard delta plain develops, the site becomes a *Taxodium* swamp and freshwater marsh (Fig. 10: Stage 2–3). Then, ~1,300BP delta lobe abandonment drove the shift from *Taxodium* swamp forest to a freshwater deltaic-lake surrounded by uneven topography.

Beginning ~700 BP, the Bayou Lafourche delta prograded to the site, resulting in a transition to an intermediate and brackish marsh. These inter-zonal shifts are all best explained as effects of the delta cycle. However, since ~200 BP the ecological shifts have been primarily driven by RSL and climatic conditions, both direct and indirect, and to a lesser degree by anthropogenic activities. The shift to a *Spartina* marsh was driven by increased salinity as a result of rising RSL, both directly due to the increasing proximity of the sea and indirectly through the increasing impact of storm surges as the shoreline retreated (Fig. 1C). Rising RSL is, of course, a result of climatic conditions in addition to subsidence. Human-generated removal of subsurface fluids (water and petroleum) and the dredging of canals and general infrastructural activities have also played a role (Monte, 1978) by permitting the landward movement of marine waters. The most recent change, the replacement of *Spartina* with black mangroves is almost entirely climate-driven, a simple response as warming temperatures drive a poleward expansion of mangroves.

6. Conclusions

A mangrove-dominated island near the landward edge of Bay Champagne near Port Fourchon, Louisiana, has experienced significant geological, geochemical, and ecological transitions over the late Holocene, due to a variety of factors, including the evolution of the Mississippi delta, climate change, sea-level rise, subsidence, tropical cyclones, and anthropogenic impacts. The site has undergone a sequence of major ecological and geochemical shifts, transitioning from a *Taxodium* freshwater swamp with elevated Ti, K, and Zr concentrations (4.0–1.3 cal yr BP), to a *Typha-Bacopa* freshwater deltaic-lake marked by elevated Mn concentrations (1.3–0.7 cal yr BP). An intermediate and brackish marsh marked by elevated Cl and Br concentrations occurred between 0.7 and 0.2 cal yr BP, then the *Typha* and *Sagittaria* communities were replaced by *Spartina*, *Salicornia*, and *Batis* as the site became a *Spartina*-dominated saline marsh with increased Sr and Cl concentrations since 0.2 cal yr BP. Although *Avicennia* has been present since the early 20th century, the establishment of a short-stature *Avicennia* forest as the dominant ecosystem has occurred only over the last few decades.

Naturally, each of the five environments in this sequence developed as a response to the ambient environment, with ecosystem changes corresponding to altered background parameters. Using PCA as a means of identifying correlations between the geochemical and ecological variables has permitted the identification of the external forcing agent(s) driving each change. The high Zr, Ti, and K concentrations associated with homogeneous fine-sand and silt suggest that intense delta progradation was the principal agent driving the creation of the *Taxodium* dominated swamp and freshwater marsh (4.0–1.3 cal yr BP). The occurrences of the terrestrial elements Ti, Mn, and K, and high Mn indicate subaqueous deposition of terrestrial sediments in a palustrine wetland, indicating that the subsidence associated with delta abandonment drove the formation of the deltaic lake (1.3–0.7 cal yr BP) environment. Elevated terrestrial elements (K, and Br) during the Bayou Lafourche delta development led to the encroachment of marshes around 0.4 cal yr BP. Peat-clastic intervals containing foraminifera (*Ammonia*) tests and the replacement of *Typha* by Poaceae (mainly *Spartina*), *Salicornia*, and *Batis* with elevated Cl concentrations around 0.2 cal yr BP indicate that a rising RSL associated with delta abandonment was the agent forcing the ecosystem shift from intermediate marsh to saltmarsh. Clastic sediments containing high carbonate contents associated with a rapid coastal retreat of the Caminada-Moreau Headland and increasing impact of storm surges indicate that a rising RSL resulting from climatic warming increased salinity at the site during the 19th century, while the most recent change, the replacement of *Spartina* with black mangroves is almost entirely climate-driven.

Although the Mississippi delta cycle has been the most important mechanism driving the ecosystem changes, other processes including hydrodynamics, hurricane, and climate change have also had significant impacts. In particular, both hurricanes and climatic

warming have been important drivers of the expansion of black mangroves. The paleoenvironmental reconstruction of coastal Louisiana is essential knowledge as understanding the response of wetland ecosystems to the full spectrum of external forcing agents is critical to determining proper coastal protection and ecological restoration measures.

Author contributions

Junghyung Ryu: Conceptualization-Lead, Data curation-Lead, Formal analysis-Lead, Investigation-Lead, Methodology-Equal, Project administration-Equal, Resources-Equal, Software-Lead, Visualization-Lead, Writing-original draft-Lead. Kam-biu Liu: Conceptualization-Equal, Formal analysis-Equal, Funding acquisition-Lead, Investigation-Equal, Methodology-Lead, Project administration-Lead, Resources-Lead, Supervision-Lead, Validation-Equal, Writing-review & editing-Lead. Terry McCloskey: Writing-review & editing-Supporting.

Declaration of competing interest

The authors confirm that there is no conflict of interest organization.

Acknowledgments

This study was supported by grants from the National Science Foundation (NSF #1759715, 1212112). We thank Cohen Marcelo Cancela Lisboa, de Souza, Adriana Vivan, and Qiang Yao for their help in the field and the laboratory.

Appendix A. Supplementary data

Supplementary data to this article can be found online at https://doi.org/10.1016/j.quascirev.2021.107292.

References

Abdi, H., Williams, L.J., 2010. Principal component analysis. Wiley Interdiscipl. Rev.: Comput. Stat. 2 (4), 433–459.
Alleman, L., Hester, M., 2011. Refinement of the fundamental niche of black mangrove (Avicennia germinans) seedlings in Louisiana: applications for restoration. Wetl. Ecol. Manag. 19 (1), 47–60.
Allison, M.A., Bianchi, T.S., McKee, B.A., Sampere, T.P., 2007. Carbon burial on river-dominated continental shelves: impact of historical changes in sediment loading adjacent to the Mississippi River. Geophys. Res. Lett. 34 (1).
Authority, C.P.a.R., 2012. Caminada Headland Beach and Dune Restoration (BA-45) Final Design Repost. *Coastal Engineering Consultants Inc*(Coastal Protection and Restoration Authority.
Blaauw, M., 2010. Methods and code for 'classical' age-modelling of radiocarbon sequences. Quat. Geochronol. 5 (5), 512–518.
Blott, S.J., Pye, K., 2001. GRADISTAT: a grain size distribution and statistics package for the analysis of unconsolidated sediments. Earth Surf. Process. Landforms 26 (11), 1237–1248.
Blum, M.D., Roberts, H.H., 2012. The Mississippi delta region: past, present, and future. Annu. Rev. Earth Planet Sci. 40, 655–683.
Bomer, E.J., Bentley, S.J., Hughes, J.E., Wilson, C.A., Crawford, F., Xu, K., 2019. Deltaic morphodynamics and stratigraphic evolution of middle Barataria Bay and middle Breton sound regions, Louisiana, USA: implications for River-Sediment Diversions. Estuar. Coast Shelf Sci. 224, 20–33.
Boonstra, M., Ramos, M., Lammertsma, E., Antoine, P., Hoorn, C., 2015. Marine connections of Amazonia: evidence from foraminifera and dinoflagellate cysts (early to middle Miocene, Colombia/Peru). Paleogeogr. Palaeoclimatol. Palaeoecol. 417, 176–194.
Briant, R.M., Bateman, M.D., 2009. Luminescence dating indicates radiocarbon age underestimation in late Pleistocene fluvial deposits from eastern England. J. Quat. Sci.: Publ. Quater. Res. Assoc. 24 (8), 916–927.
Chamberlain, E.L., Törnqvist, T.E., Shen, Z., Mauz, B., Wallinga, J., 2018. Anatomy of Mississippi Delta growth and its implications for coastal restoration. Sci. Adv. 4 (4), 4740.
Chmura, G.L., 1990. Palynological and Carbon-Isotopic Techniques for Reconstruction of Paleomarsh Salinity Zones. Doctoral dissertation. Louisiana State University, and Agricultural & Mechanical College, p. 9104120.
Christen, J.A., Pérez, S., 2009. A new robust statistical model for radiocarbon data. Radiocarbon 51 (3), 1047–1059.
Coleman, J.M., Roberts, H.H., Stone, G.W., 1998. Mississippi River delta: an overview. J. Coast Res. 699–716.
Control, C. f. D., & Prevention, 2005. Surveillance for illness and injury after hurricane katrina–new Orleans, Louisiana, September 8-25, 2005. MMWR (Morb. Mortal. Wkly. Rep.): Morb. Mortal. Wkly. Rep. 54 (40), 1018–1021.
Couvillion, B.R., Beck, H., Schoolmaster, D., Fischer, M., 2017. Land Area Change in Coastal Louisiana (1932 to 2016). US Geological Survey Report, 2329-132X.
Couvillion, B.R., Beck, H., 2013. Marsh collapse thresholds for coastal Louisiana estimated using elevation and vegetation index data. J. Coast Res. 63 (sp1), 58–67.
Croudace, I.W., Rindby, A., Rothwell, R.G., 2006. ITRAX: description and evaluation of a new multi-function X-ray core scanner. Geol. Soc. Lond. Spec. Publ. 267 (1), 51–63.
Crowley, G., Grindrod, J., Kershaw, A., 1994. Modern pollen deposition in the tropical lowlands of northeast Queensland, Australia. Rev. Palaeobot. Palynol. 83 (4), 299–327.
Dartez, S., Borne, B., Poff, M., 2020. Turning a tragedy into large-scale barrier island restoration in Louisiana: a three-project case study. Shore Beach 88 (1), 58–64.
Day, J.W., Boesch, D.F., Clairain, E.J., Kemp, G.P., Laska, S.B., Mitsch, W.J., Orth, K., Mashriqui, H., Reed, D.J., Shabman, L., 2007. Restoration of the Mississippi delta: lessons from hurricanes Katrina and Rita. Science 315 (5819), 1679–1684.
Dean, J.W.E., 1974. Determination of carbonate and organic matter in calcareous sediments and sedimentary rocks by loss on ignition: comparison with other methods. J. Sediment. Res. 44 (1).
DeWitt, N.T., Flocks, J.G., Hansen, M., Kulp, M., Reynolds, B., 2007. Bathymetric survey of the nearshore from Belle Pass to Caminada Pass, Louisiana: methods and data report. US Geol Surv Data Series 312.
Dietz, M., Liu, K., Bianchette, T., 2018. Hurricanes as a major driver of coastal erosion in the Mississippi River delta: a multi-decadal analysis of shoreline retreat rates at bay Champagne, Louisiana (USA). Water 10, 1480.
Dill, H.G., 2010. The "chessboard" classification scheme of mineral deposits: mineralogy and geology from aluminum to zirconium. Earth Sci. Rev. 100 (1–4), 1–420.
Donahoe, R., Liu, C., Dobson, K., Graham, E., 1994. Cycling of iron and manganese in a Riparian wetland. Mineral. Mag. 58 (1), 237–238.
Elliott, T., 1986. Chapter 6. Deltas. Sedimentary Environments and Facies, second ed. Blackwell, Oxford, UK, pp. 155–188.
Faegri, K., Iversen, J., Waterbolk, H., 1964. Textbook of Pollen. *Analysis*. Hafner Publishing Co., NY.
Faegri, K., Kaland, P.E., Krzywinski, K., 1989. Textbook of Pollen Analysis. John Wiley & Sons Ltd.
Flannery, J.A., 2008. Graduate Theses and Dissertations. A 1400 Year Multi-Proxy Record of Hydrologic Variability in the Gulf of Mexico: Exploring Ocean-Continent Linkages during the Late Holocene, vol. 241. The University of South Florida.
Flocks, J.G., Ferina, N.F., Dreher, C., Kindinger, J.L., FitzGerald, D.M., Kulp, M.A., 2006. High-resolution stratigraphy of a Mississippi subdelta-lobe progradation in the Barataria bight, north-Central Gulf of Mexico. J. Sediment. Res. 76 (3), 429–443.
Frazier, D.E., 1967. Recent deltaic deposits of the Mississippi River: their development and chronology. Gulf Coast Assoc. Geol. Soc. Trans. 17, 287–315.
Gee, G.W., Or, D., 2002. Methods of soil analysis. Part 4. 2.4 Particle-size Analysis, vol. 598, pp. 255–293.
Gerdes, R.G., 1982. Stratigraphy and History of Development of the Caminada-Moreau Beach Ridge Plain (southeast Louisiana).
Godwin, H., 1934. Pollen analysis. An outline of the problems and potentialities of the method. New Phytol. 33 (5), 325–358.
Gonzalez, J.L., Törnqvist, T.E., 2009. A new Late Holocene sea-level record from the Mississippi Delta: evidence for a climate/sea level connection? Quat. Sci. Rev. 28 (17–18), 1737–1749.
Guntenspergen, G.R., Cahoon, D.R., Grace, J., Steyer, G.D., Fournet, S., Townson, M., Foote, A.L., 1995. Disturbance and recovery of the Louisiana coastal marsh landscape from the impacts of Hurricane Andrew. J. Coast Res. 324–339.
Hicks, S., Birks, H., 1996. Numerical analysis of modern and fossil pollen spectra as a tool for elucidating the nature of fine-scale human activities in boreal areas. Veg. Hist. Archaeobotany 5 (4), 257–272.
Hijma, M.P., Shen, Z., Törnqvist, T.E., Mauz, B., 2017. Late Holocene evolution of a coupled, mud-dominated delta plain–chenier plain system, coastal Louisiana, USA. Earth Surf. Dynam. 5 (4), 689.
Hutley, L.B., Evans, B.J., Beringer, J., Cook, G.D., Maier, S.W., Razon, E., 2013. Impacts of an extreme cyclone event on landscape-scale savanna fire, productivity and greenhouse gas emissions. Environ. Res. Lett. 8 (4), 045023.
Jankowski, K.L., Törnqvist, T.E., Fernandes, A.M., 2017. Vulnerability of Louisiana's coastal wetlands to present-day rates of relative sea-level rise. Nat. Commun. 8, 14792.
Jiang, J., DeAngelis, D.L., Anderson, G.H., Smith, T.J., 2014. Analysis and simulation of propagule dispersal and salinity intrusion from storm surge on the movement of a marsh–mangrove ecotone in South Florida. Estuar. Coast 37 (1), 24–35.
Juggins, S., 2007. C2: Software for Ecological and Palaeoecological Data Analysis and Visualization (User Guide Version 1.5). Newcastle upon Tyne. Newcastle University, p. 77.
Kiage, L.M., 2019. A 1200-year history of environmental changes in Bay Jimmy area, coastal Louisiana, USA. Holocene 30 (2), 201–209.
Kindinger, J., Flocks, J., Kulp, M., Penland, S., Britsch, L.D., Brewer, G., Brooks, G.L.,

Dadisman, S., Dreher, C., Ferina, N., 2001. Sand Resources, Regional Geology, and Coastal Processes for the Restoration of the Barataria Barrier Shoreline. Report to U.S. Army Corps of Engineers, New Orleans District, 2331-1258.
Kindinger, J.L., Buster, N.A., Flocks, J.G., Bernier, J.C., Kulp, M.A., 2013. Louisiana Barrier Island Comprehensive Monitoring (BICM) Program Summary Report: Data and Analyses 2006 through 2010. US Department of the Interior, US Geological Survey.
Kolb, C.R., Van Lopik, J.R., 1966. Depositional environments of the Mississippi River deltaic plain—southeastern Louisiana. AAPG (Am. Assoc. Pet. Geol.) Bull. 49 (10), 1755-1755.
Kolb, C.R., a, V.L., J, R., 1958. Geology Of the Mississippi River Deltaic Plain, Southeastern Louisiana: Volume 1. Waterways Experiment Station (U.S.): Vicksburg, Miss. Army Engineer Waterways Experiment Station, p. 1958.
Kosters, E., Chmura, G., Bailey, A., 1987. Sedimentary and botanical factors influencing peat accumulation in the Mississippi Delta. J. Geol. Soc. 144 (3), 423–434.
Krauss, K.W., McKee, K.L., Hester, M.W., 2014. Water use characteristics of black mangrove (Avicennia germinans) communities along an ecotone with marsh at a northern geographical limit. Ecohydrology 7 (2), 354–365.
Levin, D.R., 1990. Transgressions and Regressions in the Barataria Bight Region of Coastal Louisiana. Louisiana State University, p. 5072. LSU Historical Dissertations and Theses.
Levin, D.R., 1991. Transgressions and regressions in the Barataria Bight region of coastal Louisiana. Gulf Coast Assoc. Geol. Soc. Trans. 41, 408–431.
Liu, K., 1990. Holocene paleoecology of the boreal forest and Great lakes-St. Lawrence forest in northern Ontario. Ecol. Monogr. 60 (2), 179–212.
Liu, K., Fearn, M.L., 2000. Holocene History of Catastrophic Hurricane Landfalls along the Gulf of Mexico Coast Reconstructed from Coastal Lake and Marsh Sediments. Current Stresses and Potential Vulnerabilities: Implications of Global Change for the Gulf Coast Region of the United States. Franklin Press, p. 223.
Liu, K., Lu, H., Shen, C., 2008. A 1200-year proxy record of hurricanes and fires from the Gulf of Mexico coast: testing the hypothesis of hurricane–fire interactions. Quat. Res. 69 (1), 29–41.
Liu, K., McCloskey, T.A., Bianchette, T.A., Keller, G., Lam, N.S., Cable, J.E., Arriola, J., 2014. Hurricane Isaac storm surge deposition in a coastal wetland along Lake Pontchartrain, southern Louisiana. J. Coast Res. 70 (sp1), 266–271.
Malacara, D., 2011. Color Vision and Colorimetry: Theory and Applications. Publisher, Spie Bellingham, WA.
McAndrews, J.H., Berti, A.A., Norris, G., 1973. Key to the Quaternary Pollen and Spores of the Great Lakes Region. Royal Ontario Museum: Life Science, pp. 1–63.
McCloskey, T.A., Smith, C.G., Liu, K., Marot, M., Haller, C., 2017. How could a freshwater swamp produce a chemical signature characteristic of a saltmarsh? ACS Earth Space Chem. 2 (1), 9–20.
McCloskey, T.A., Smith, C.G., Liu, K., Nelson, P.R., 2018. The effects of tropical cyclone-generated deposition on the sustainability of the Pearl River Marsh, Louisiana: the importance of the geologic framework. Front. Ecol. Evol. 6, 179.
Monte, Judith Ann, 1978. The Impact of Petroleum Dredging on Louisiana's Coastal Landscape: a Plant Biogeographical Analysis and Resource Assessment of Spoil Bank Habitats in the Bayou Lafourche Delta. LSU Historical Dissertations and Theses, p. 3291.
Morgan, J.P., Larimore, P.B., 1957. Changes in the Louisiana shoreline. Gulf Coast Assoc. Geol. Soc. Trans. 7, 303–310.
Montagna, P.A., Gibeaut, J.C., Tunnell Jr., J.W., 2007. South Texas climate 2100: coastal impacts. In: South Texas Climate, vol. 2100, pp. 57–77.
Naquin, J.D., Liu, K., McCloskey, T.A., Bianchette, T.A., 2014. Storm deposition induced by hurricanes in a rapidly subsiding coastal zone. J. Coast Res. 70 (sp1), 308–313.
Nittrouer, C., Sternberg, R., 1981. The formation of sedimentary strata in an allochthonous shelf environment: the Washington continental shelf. Mar. Geol. 42 (1–4), 201–232.
Nriagu, J., Dell, C., 1974. Diagenetic formation of iron phosphates in recent lake sediments. Am. Mineral.: J. Earth Planet. Mater. 59 (9–10), 934–946.
O'Neil, T., 1949. The Muskrat in the Louisiana Coastal Marshes: A Study of the Ecological, Geological, Biological, Tidal and Climatic Factors Governing the Production and Management of the Muskrat Industry in Louisiana: Federal Aid Section, Fish and Game Division. Louisiana Dept. of Wild Life. Oct 10.
Osland, M.J., Day, R.H., Hall, C.T., Brumfield, M.D., Dugas, J.L., Jones, W.R., 2017. Mangrove expansion and contraction at a poleward range limit: climate extremes and land-ocean temperature gradients. Ecology 98 (1), 125–137.
Osland, M.J., Day, R.H., Hall, C.T., Feher, L.C., Armitage, A.R., Cebrian, J., Dunton, K.H., Hughes, A.R., Kaplan, D.A., Langston, A.K., 2020a. Temperature thresholds for black mangrove (Avicennia germinans) freeze damage, mortality and recovery in North America: refining tipping points for range expansion in a warming climate. J. Ecol. 108 (2), 654–665.
Osland, M.J., Day, R.H., Michot, T.C., 2020b. Frequency of extreme freeze events controls the distribution and structure of black mangroves (*Avicennia germinans*) near their northern range limit in coastal Louisiana. Divers. Distrib. 26, 1366–1382.
Osland, M.J., Enwright, N., Day, R.H., Doyle, T.W., 2013. Winter climate change and coastal wetland foundation species: salt marshes vs. mangrove forests in the southeastern United States. Global Change Biol. 19 (5), 1482–1494.
Patterson, C.S., Mendelssohn, I.A., 1991. A comparison of physicochemical variables across plant zones in a mangal/salt marsh community in Louisiana. Wetlands 11 (1), 139–161.
Patterson, C.S., Mendelssohn, I.A., Swenson, E.M., 1993. Growth and survival of Avicennia germinans seedlings in a mangal/salt marsh community in Louisiana, USA. J. Coast Res. 801–810.
Penfound, W.T., Hathaway, E.S., 1938. Plant communities in the marshlands of southeastern Louisiana. Ecol. Monogr. 8 (1), 1–56.
Penland, S., Boyd, R., Suter, J.R., 1988. Transgressive depositional systems of the Mississippi delta plain: a model for barrier shoreline and shelf sand development. J. Sediment. Res. 58 (6), 932–949.
Penland, S., Connor Jr., P.F., Beall, A., Fearnley, S., Williams, S.J., 2005. Changes in Louisiana's shoreline: 1855–2002. J. Coast Res. 7–39.
Perry, C.L., Mendelssohn, I.A., 2009. Ecosystem effects of expanding populations of Avicennia germinans in a Louisiana salt marsh. Wetlands 29 (1), 396–406.
Pongrac, P., Fischer, S., Thompson, J.A., Wright, G., White, P.J., 2020. Early responses of Brassica oleracea roots to zinc supply under sufficient and sub-optimal phosphorus supply. Front. Plant Sci. 10, 1645.
Raynie, R.C., Khalil, S.M., Villarrubia, C., Haywood, E., 2020. Coastal monitoring and data management for restoration in Louisiana. Shore Beach 88 (1), 92–101.
Roberts, H.H., 1997. Dynamic changes of the Holocene Mississippi River delta plain: the delta cycle. J. Coast Res. 605–627.
Rodrigues, E., Cohen, M.C.L., Liu, K.-b., Pessenda, L.C.R., Yao, Q., Ryu, J., Rossetti, D., de Souza, A., Dietz, M., 2021. The effect of global warming on the establishment of mangroves in coastal Louisiana during the Holocene. Geomorphology 381, 107648.
Roth, D., 2010. Louisiana Hurricane History. National Weather Service Camp Springs, MD.
Rothwell, R.G., Rack, F.R., 2006. New techniques in sediment core analysis: an introduction. Geol. Soc. Lond. Spec. Publ. 267 (1), 1–29.
Ryu, J., Bianchette, T.A., Liu, K., Yao, Q., Maiti, K.D., 2018. Palynological and geochemical records of environmental changes in a Taxodium swamp near Lake Pontchartrain in southern Louisiana (USA) during the last 150 years. J. Coast Res. 85 (Special Issue), 381–385.
Ryu, J., Liu, K., Bianchette, T.A., 2021a. Holocene environmental history of a freshwater wetland in southern Louisiana: a sedimentary record of delta development, coastal evolution and human activity. J. Quat. Sci. 36, 980–990. https://doi.org/10.1002/jqs.3324.
Ryu, J., Liu, K., Bianchette, T.A., McCloskey, T., 2021b. Identifying forcing agents of environmental change and ecological response on the Mississippi River Delta, Southeastern Louisiana. Sci. Total Environ. 794, 148730.
Saucier, R.T., 1968. Recent Geomorphic History of the Pontchartrain Basin, Louisiana. Louisiana State University and Agricultural & Mechanical College, p. 1418. LSU Historical Dissertations and Theses.
Saucier, R.T., 1994. Geomorphology and Quaternary Geologic History of the Lower Mississippi Valley, ume 2. US Army Engineer Waterways Experiment Station.
Schaller, T., Wehrli, B., 1996. Geochemical-focusing of manganese in lake sediments—an indicator of deep-water oxygen conditions. Aquat. Geochem. 2 (4), 359–378.
Shankman, D., Drake, L.G., 1990. Channel migration and regeneration of bald cypress in western Tennessee. Phys. Geogr. 11 (4), 343–352.
Shen, Z., Törnqvist, T.E., Mauz, B., Chamberlain, E.L., Nijhuis, A.G., Sandoval, L., 2015. Episodic overbank deposition as a dominant mechanism of floodplain and delta-plain aggradation. Geology 43 (10), 875–878.
Sherrod, C.L., McMillan, C., 1985. The Distributional History and Ecology of Mangrove Vegetation along the Northern Gulf of Mexico Coastal Region. Texas A&M University, Galveston Campus, DSpace Repository, Galveston Bay Information Collection.
Shirazi, M.A., Boersma, L., 1984. A unifying quantitative analysis of soil texture 1. Soil Sci. Soc. Am. J. 48 (1), 142–147.
Shirazi, M.A., Hart, J.W., Boersma, L., 1988. A unifying quantitative analysis of soil texture: improvement of precision and extension of scale. Soil Sci. Soc. Am. J. 52 (1), 181–190.
Stuiver, M., Reimer, P.J., Bard, E., Beck, J.W., Burr, G.S., Hughen, K.A., Kromer, B., McCormac, G., Van Der Plicht, J., Spurk, M., 1998. INTCAL98 radiocarbon age calibration, 24,000–0 cal BP. Radiocarbon 40 (3), 1041–1083.
Sugita, S., 1993. A model of pollen source area for an entire lake surface. Quat. Res. 39 (2), 239–244.
Talma, A., Vogel, J.C., 1993. A simplified approach to calibrating 14 C dates. Radiocarbon 35 (2), 317–322.
Törnqvist, T.E., Paola, C., Parker, G., Liu, K.-b., Mohrig, D., Holbrook, J.M., Twilley, R.R., 2007. Comment on" wetland sedimentation from hurricanes Katrina and Rita. Science 316 (5822), 201-201.
Törnqvist, T.E., Wallace, D.J., Storms, J.E., Wallinga, J., Van Dam, R.L., Blaauw, M., Derksen, M.S., Klerks, C.J., Meijneken, C., Snijders, E.M., 2008. Mississippi Delta subsidence primarily caused by compaction of Holocene strata. Nat. Geosci. 1 (3), 173.
Törnqvist, T.r.E., González, J.L., Newsom, L.A., Van der Borg, K., De Jong, A.F., Kurnik, C.W., 2004. Deciphering Holocene sea-level history on the US Gulf coast: a high-resolution record from the Mississippi delta. Geol. Soc. Am. Bull. 116 (7–8), 1026–1039.
Turner, R.E., Baustian, J.J., Swenson, E.M., Spicer, J.S., 2006. Wetland sedimentation from hurricanes Katrina and Rita. Science 314 (5798), 449–452.
Tweel, A.W., Turner, R.E., 2012. Landscape-scale analysis of wetland sediment deposition from four tropical cyclone events. PLoS One 7 (11).
Twilley, R., Day, J., Bevington, A., Castañeda-Moya, E., Christensen, A., Holm, G., Heffner, L., Lane, R., McCall, A., Aarons, A., 2019. Ecogeomorphology of coastal deltaic floodplains and estuaries in an active delta: insights from the

Atchafalaya Coastal Basin. Estuar. Coast Shelf Sci. 227, 106341.
Watts, W.A., Winter, T.C., 1966. Plant macrofossils from Kirchner Marsh, Minnesota—a paleoecological study. Geol. Soc. Am. Bull. 77 (12), 1339–1359.
Webb, P., 2019. Introduction to Oceanography, vol. 1. Rebus Community. Pressbooks under a CC BY (Attribution).
Wells, P.V., 1976. Macrofossil analysis of wood rat (Neotoma) middens as a key to the Quaternary vegetational history of arid America. Quat. Res. 6 (2), 223–248.
Wickham, H., Averick, M., Bryan, J., Chang, W., McGowan, L.D.A., François, R., Grolemund, G., Hayes, A., Henry, L., Hester, J., 2019. Welcome to the tidyverse. J. Open Source Softw. 4 (43), 1686.
Willard, D.A., Bernhardt, C.E., Weimer, L., Cooper, S.R., Gamez, D., Jensen, J., 2004. Atlas of pollen and spores of the Florida Everglades. Palynology 28 (1), 175–227.
Wilson, C.A., Allison, M.A., 2008. An equilibrium profile model for retreating marsh shorelines in southeast Louisiana. Estuar. Coast Shelf Sci. 80 (4), 483–494.
Wodehouse, R.P., 1937. Pollen grains: their structure, identification and significance in science and medicine. J. Nerv. Ment. Dis. 86 (1), 104.
Xu, K., Sanger, D., Riekerk, G., Crowe, S., Van Dolah, R.F., Wren, P.A., Ma, Y., 2014. Seabed texture and composition changes offshore of Port Royal Sound, South Carolina before and after the dredging for beach nourishment. Estuar. Coast Shelf Sci. 149, 57–67.
Yao, Q., Liu, K., Platt, W.J., Rivera-Monroy, V.H., 2015. Palynological reconstruction of environmental changes in coastal wetlands of the Florida Everglades since the mid-Holocene. Quat. Res. 83 (3), 449–458.